

## REPORT DOCUMENTATION PAGE

Form Approved  
OMB No. 0704-0188

Public reporting burden for this collection of information is estimated to average 1 hour per response, including the time for reviewing instructions, searching existing data sources, gathering and maintaining the data needed, and completing and reviewing the collection of information. Send comments regarding this burden estimate or any other aspect of this collection of information, including suggestions for reducing this burden, to Washington Headquarters Services, Directorate for Information Operations and Reports, 1215 Jefferson Davis Highway, Suite 1204, Arlington, VA 22202-4302, and to the Office of Management and Budget, Paperwork Reduction Project (0704-0188), Washington, DC 20503.

1. AGENCY USE ONLY (Leave blank)	2. REPORT DATE	3. REPORT TYPE AND DATES COVERED
	June 7, 1995	August 1, 1992 to January 15, 1995

4. TITLE AND SUBTITLE	5. FUNDING NUMBERS
Direct Numerical Simulation of Acoustic-Flow Interactions in Solid Rocket Motors	F49620-92-J-0451

6. AUTHOR(S)	AFOSR-TR-95
S. Mu, S. Hevert, and S. Mahalingam	0532

7. PERFORMING ORGANIZATION NAME(S) AND ADDRESS(ES)	153-7118
The Regents of the University of Colorado Campus Box 19 Boulder, CO 80309-0019	

9. SPONSORING / MONITORING AGENCY NAME(S) AND ADDRESS(ES)	10. SPONSORING / MONITORING AGENCY REPORT NUMBER
Air Force Office of Scientific Research Bolling Air Force Base, DC, 20332-6448	NA F49620-92- J-0451

11. SUPPLEMENTARY NOTES	
12a. DISTRIBUTION / AVAILABILITY STATEMENT	12b. DISTRIBUTION CODE
Approved for public release, distribution unlimited	

13. ABSTRACT (Maximum 200 words)
A summary of research on our studies of acoustic-mean flow interactions in solid rocket motors is presented in this Final Technical Report. Two-dimensional, time-dependent solutions of the compressible Navier-Stokes equations have been obtained in a rectangular duct under conditions of monochromatic acoustic forcing. The existence of a cut-off frequency, the appearance of oblique waves, and the behavior at resonance compare well with previously published analytical predictions. The thickness of the acoustic boundary layer and its response to imposed disturbances are also in good agreement with theory. The code is being modified to include nonpremixed combustion, which will allow studying acoustic interactions with a chemically reactive mean flow.

14. SUBJECT TERMS	15. NUMBER OF PAGES		
	41		
	16. PRICE CODE		
17. SECURITY CLASSIFICATION OF REPORT	18. SECURITY CLASSIFICATION OF THIS PAGE	19. SECURITY CLASSIFICATION OF ABSTRACT	20. LIMITATION OF ABSTRACT
UNLIMITED	U	U	U

Standard Form 298 (Rev. 2-89)

19950821 056

DTIC QUALITY INSPECTED 2

# **Direct Numerical Simulation of Acoustic-Flow Interactions in Solid Rocket Motors**

**Siming Mu, Stephen Hevert and Shankar Mahalingam**

**Final Technical Report  
AFOSR Grant No. F49620-92-J-0451  
Contract Monitor: Dr. Mitat Birkan**

**June 7, 1995**

**CCR Report No. 95-02**

**Center for Combustion Research  
Department of Mechanical Engineering  
University of Colorado at Boulder  
Boulder, CO 80309-0427**

## ABSTRACT

A summary of research on our studies of acoustic-mean flow interactions in solid rocket motors is presented in this Final Technical Report. The objective of this research was to study the effects of acoustic refraction on the mean flow with imposed acoustic disturbances of various frequencies. The interaction between an imposed monochromatic, time-dependent acoustic disturbance and a steady mean shear flow in a two-dimensional duct was studied using direct numerical simulation. Unlike previously reported numerical results, the long time acoustic response is captured through implementation of accurate non-reflecting boundary conditions. Below a certain cut-off frequency, the acoustic field is a nearly planar traveling wave propagating axially along the duct. Above this cut-off frequency, oblique waves are generated due to both acoustic refraction and cross-stream dependent source oscillation, leading to an alternating pattern of higher acoustic pressures at the wall and the centerline, downstream of the disturbance source. At resonant conditions, the growth of the oblique wave, which is nearly transverse, dominates the axial wave, leading to a phase change of 180 degrees after their interaction. The thickness of the acoustic boundary layer and its response to imposed disturbances are also in good agreement with theory. These results are consistent with previously published theoretical predictions, and represent their first numerical verification. The code is being modified to include nonpremixed combustion, which will allow studying acoustic interactions with a chemically reactive mean flow. The manuscript in the Appendix is to appear in the AIAA Journal either in 1995 or 1996, and represents most of the work done in connection with this contract.

Accession For	
NTIS GRA&I	<input checked="" type="checkbox"/>
DTIC TAB	<input type="checkbox"/>
Unannounced	<input type="checkbox"/>
Justification	
By	
Distribution/	
Availability Codes	
Dist	Avail 8 d/s
	Special

A-1

## Table of Contents

Table of Contents .....	ii
1. INTRODUCTION AND RESEARCH OBJECTIVES .....	1
2. DIRECT NUMERICAL SIMULATION PROCEDURE .....	1
3. PROGRESS TO DATE .....	2
4. FUTURE PLANS .....	5
5. REFERENCES .....	5
6. PERSONNEL .....	6
7. PUBLICATIONS .....	6
APPENDIX .....	18

## 1. INTRODUCTION AND RESEARCH OBJECTIVES

Combustion-driven acoustic instabilities in solid rocket motors arise as a result of a complex interaction between the acoustics of the flow field and oscillations in propellant burning rate. The net energy associated with acoustic instabilities is determined by a balance of competing processes that feed and extract energy from the acoustic field. The relative importance of these processes is strongly dependent on both the mode of oscillation and type of propellant, thus making it difficult to isolate physical mechanisms associated with individual processes when the problem is studied as a whole.

The focus of the present research is on the effects of acoustic refraction caused by the interaction of disturbances imposed on a viscous mean flow through a two dimensional channel. This is accomplished through Direct Numerical Simulation (DNS) of the flow field in several model problems tailored to address specific features of the interaction between the mean flow and the acoustic disturbances. The overall objective is to develop a methodology that will allow one to extract acoustic information from data generated through DNS. It is expected that this process will lead to a better understanding of acoustic-mean flow interactions in solid rocket motors. Our specific objective is to validate the numerical simulations with analytical results obtained by Wang and Kassoy (1991), thereby developing and fine tuning a procedure that can be used to track energy in the mean flow for various acoustic modes of oscillation. To date, we have modified an existing DNS computer code and have obtained results for unsteady flow in a rectangular duct. The DNS procedure is described in Section 2. Our progress to date is presented in Section 3. Finally, an outline of our future research plans is provided in Section 4.

## 2. DIRECT NUMERICAL SIMULATION PROCEDURE

A direct numerical simulation code for 2D compressible flow developed by Baum (1993) was modified and is used in our investigations. The continuity, momentum and energy equations for compressible flow are solved numerically. Pressure, density, and temperature are related through the ideal gas equation of state. The specific heats are presumed constant and fluid properties such as dynamic viscosity and thermal conductivity are assumed to be functions of temperature. The equations are solved using a sixth-order accurate compact finite difference scheme (Lele, 1992) for evaluating spatial derivatives. Time advancement is achieved through a third-order accurate Runge-Kutta scheme. The Navier Stokes Characteristic Boundary Condition (NSCBC) procedure developed by Poinsot and Lele (1992) is used to implement boundary conditions at the lateral and streamwise edges of the computational domain.

Figure 1 is a schematic representation of our computational domain and coordinate system definition. The aspect ratio is defined as  $L/2h$ . The grid spacing in the computational mesh is varied depending on the computational resolution required, and to evaluate the sensitivity of the analysis to grid spacing. The equations are cast in dimensionless form and time-advanced to obtain either steady or unsteady solutions. The duct length  $L$ , the speed of sound in the far

field  $c_\infty$ , and a characteristic acoustic time, based on  $L$  and  $c_\infty$  are used as reference length, velocity, and time scales. Other variables are rendered dimensionless by their properties in the far field.

### 3. PROGRESS TO DATE

As reported previously, several test cases were run to validate the modifications that were made to the 2D code, including the behavior of the nonreflecting boundary conditions, and the overall behavior of the code for stability and convergence. A critical requirement for accurately capturing acoustic wave structure is a nonreflecting outlet boundary, where waves generated at the inlet can pass through with little or no reflection back into the computational domain.

After validating the boundary condition treatment and the numerical scheme, perturbations were imposed on the inlet axial velocity. In order to compare numerical results with the analytical results of Wang and Kassoy (1992), it is necessary to impose a plane wave (constant amplitude) disturbance. However it is not possible to implement this form of perturbation in the numerical simulation because of the no slip condition that is required at the lateral boundaries. The actual form of the disturbance used in the simulation is shown in Figure 2, and is mathematically expressed as

$$\hat{u} = AU(y) \sin[5\pi(y + 0.1)] \sin(\Omega t), \quad (1)$$

where  $\hat{u}$  is the axial velocity disturbance,  $\Omega$  is the dimensionless frequency of the disturbance defined through  $\Omega = \Omega' L/a$ , where  $\Omega'$  is the dimensional frequency, and  $a$  is the speed of sound. The advantage of this amplitude structure is that it does not introduce any discontinuity or sharp gradients so that relatively large values for  $A$  may be used. Also, by performing a Fast Fourier Transform (FFT) in  $y$  for a discrete representation of Equation 1, it is found that the dominant transverse spatial components are the zeroth and first modes, with higher modes being negligibly small.

With an expression for the imposed disturbance of the axial velocity specified, the acoustic pressure field under various driving frequencies was studied. Several values of angular frequency were considered. Guided by the work of Wang and Kassoy (1992), these values were chosen to represent typical characteristics of different frequency regimes. In all cases, the computations were performed for up to four acoustic time units, as compared to only one acoustic time unit in previous numerical simulations.

1. *Acoustic pressure field for  $\Omega = 10$ .* This is the lowest frequency studied in the simulations, and corresponds to the dimensionless frequency  $\Omega_w = 2$  used in the analysis of Wang and Kassoy (1992). Figures 3(a) and (b) represent the total acoustic pressure time history and pressure contours at the indicated locations. Notice that in Figure 3(a) the amplitude of

the acoustic pressure at the centerline is slightly smaller than that at the wall. This is a consequence of acoustic refraction that deflects the acoustic waves toward the boundaries. The constant wave amplitude shown in Figure 3(a) indicates that the only wave existing in the duct is that imposed at the inlet. The contour plot in Figure 3(b) confirms this by showing that the acoustic pressure gradient is primarily in the axial direction.

2. *Acoustic pressure field for  $\Omega = 40$ .* The acoustic pressure time history at fixed locations is presented in Figure 4 for a dimensionless forcing frequency  $\Omega = 40$ . Compared with Figure 3(a), it reveals several interesting features. Initially, after the arrival of the acoustic waves, an increase in their amplitudes is observed. The amplitudes then start to oscillate over time. This variation in amplitude can be explained by the analytical work of Wang and Kassoy (1992). They identified a cutoff frequency  $\Omega = 5n\pi, n = 1, 2, 3, \dots$  below which the waves remain planar in the duct. For a plane wave with  $\Omega$  above  $10\pi$ , oblique waves are generated as the disturbance moves downstream. The path of the oblique waves can be traced by examining the acoustic pressure contours in Figure 5. The direction of the maximum pressure gradient is an indication of the direction the waves propagate. The wave front is aligned normal to this direction. The intersection between the developing oblique waves and the axially travelling waves results in the variation of amplitude.

Another important result may be obtained by examining the acoustic pressure time history along the wall and at the centerline at several streamwise stations. These data are presented in Figure 6. A consequence of acoustic refraction due to shear flow interaction is that the acoustic pressure is higher at the wall than at the centerline for downstream propagating waves. However, in the presence of oblique waves this is not true everywhere in the domain. Instead, by studying Figures 5 and 6, one notes that higher acoustic pressure exists only in those places where oblique waves pass through. This further indicates the importance of oblique waves in the study of the acoustic field.

3. *Acoustic pressure field for  $\Omega = 10\pi$ .* This angular frequency corresponds to the second resonant mode of the channel. Figures 7(a)-(h) depicts the acoustic pressure time history at the centerline and at the wall at different axial locations along the channel. The general feature of the resonant oscillation is displayed at locations (1c) and (1w), where the acoustic pressure amplitudes increase with time. Figures 7(b) and (c) depict slightly different features. One can observe that at some locations the signal initially decreases and subsequently increases. A similar behavior is presented in Wang and Kassoy (1992). More interesting behavior can be seen further downstream. After the initial decrease in amplitude due to destructive interference, the wave amplitudes at all locations start to increase with time. Then at some locations the wave amplitudes remain nearly constant, suggesting that acoustic energy due to resonant oscillations is somehow being transferred out of the acoustic field at these locations. However, at other locations the wave amplitudes start to decrease and eventually reach a value close to zero. After that, the pressure

amplitudes increase once again having undergone a phase change of  $\pi$  with respect to the phase at the inlet. This phase change is illustrated in Figure 8, where data from locations (6c) and (6w) have been overlaid. A similar behavior was suggested by Wang and Kassoy (1992); however, since previous numerical simulations were limited to a few wave cycles only, the results had not been verified. The present numerical simulations overcome this limitation, and the results show good qualitative agreement with analytical predictions.

*Acoustic Boundary Layer Analysis.* The existence of an acoustic boundary layer is another interesting feature that arises due to the acoustic-mean flow interaction. Represented in Figures 9(a)-(e), it is the region close to the wall within which an overshoot of axial acoustic velocity can be observed. The magnitude of the overshoot reaches a maximum value whenever the axial velocity in the core changes sign. This effect is called *Richardson's annular effect* (Baum and Levine, 1978, and Wang and Kassoy, 1992). The thickness of the acoustic boundary layer is given in analytical form by

$$\delta = 5 \left( \frac{M}{\Omega Re} \right)^{1/2} \quad (2)$$

where  $M$  is the maximum centerline Mach number and  $Re$  is the Reynolds number based on the centerline velocity and duct width. For the field shown in Figures 9(a)-(e) with  $Re = 320$  and  $M \approx 0.8$ , Equation 2 predicts an acoustic boundary layer thickness of 5.6

*Preliminary Results for Flow with Sidewall Injection.* For this simulation, the left boundary of the computational domain is closed; i.e., flow is not permitted through the boundary. Flow through the channel is generated by specifying mass injection from the lateral boundaries along  $y = \pm h$  (see Figure 1). The boundary conditions imposed are (1)  $u = v = 0, T = \text{const.}$  along  $x = 0$ , (2) nonreflecting boundary at outlet, and (3)  $u = 0, v = \pm V_0, T = \text{const.}$  along  $y = \pm h$ , where  $V_0$  is the magnitude of the injection velocity, taken to be 0.01 in the present simulation. Figures 10(a) and (b) show the comparison between the numerical and inviscid analytical steady flow model. The difference between the two are probably due to the viscous nature of the fluid assumed in the numerical simulation.

After the steady state is obtained, a small pressure disturbance is imposed at the outlet through

$$p_{\text{total,outlet}} = p_{\text{steady,outlet}} + \varepsilon \hat{p} \quad (3)$$

where  $\varepsilon$  is a asymptotic parameter taking the value 0.01 and

$$\hat{p} = A \sin(\Omega t) \quad (4)$$

where  $A$ , the magnitude of the disturbance, is taken as the steady state pressure at the center of the outlet. Dimensionless frequencies assumed in the analysis were  $\Omega = 5, 10, 10\pi, 40$ . The vortical component of the axial velocity is obtained through the following relation suggested by Price and Flandro (1992) and Zhao, *et. al.* (1994):

$$u_{\text{vortical}} = u_{\text{total}} - u_{\text{steady}} - u_{\text{center}} \quad (5)$$

Figure 11 represents the comparison between  $u_{\text{vortical}}$  profiles for the different frequencies. The acoustic boundary layer is extended towards the core region of flow due to the convective effect of mass injection. However, the thickness of this layer is still dependent on the frequency as it is in the case for flow without mass injection.

#### 4. FUTURE WORK

We are currently enhancing the 2D code in order to simulate a 2D nonpremixed flame confined between the walls of a narrow horizontal duct with open ends. Single step, finite rate chemistry is assumed for the combustion process, with the unmixed reactants diffusing into the flame zone from opposite sides of the channel. Eventually one end of the channel will be closed, and acoustic perturbations will be imposed on the reacting flow field. This is the first step toward modeling the effects of acoustics on the combustion response of a nonpremixed flame confined near the surface of a burning propellant. In the future, this analysis will be extended to simulate the response of a premixed flame adjacent to the burning propellant.

#### 5. REFERENCES

1. BAUM, J. D. AND J. N. LEVINE, "Numerical Techniques for Solving Nonlinear Instability Problems in Solid Rocket Motors," AIAA Journal, **20**(7), 955-961, (1982).
2. BAUM, J. D. AND J. N. LEVINE, "Numerical Investigation of Acoustic Refraction," AIAA Journal, **25**(12), 1577-1586, (1987).
3. FLANDRO, G. A. AND R. L. ROACH, "Effects of Vorticity Production on Acoustic Waves in A Combustion Chamber," Final Technical Report AFOSR-90-0159, (1992).
4. BAUM, M., Ph.D thesis, Ecole Centrale de Paris, 1993.
5. LELE, S. K., "Compact finite difference schemes with spectral-like accuracy," J. Comp. Phys., **103**, 16-42, 1992.
6. POINSOT, T. AND S. LELE, "Boundary conditions for direct simulations of compressible viscous flows," J. Comp. Phys., **101**, 104-129, 1992.

7. PRICE, E. W., AND G. A. FLANDRO, "Combustion Instability in Solid Propellant Rockets," Book manuscript in preparation, 1993.
8. THOMPSON, K., "Time-dependent boundary conditions for hyperbolic systems, II," J. Comp. Phys., 89, 439-461, 1990.
9. VUILLOT, F. AND G. AVALON, "Acoustic Boundary Layers in Solid Propellant Rocket Motors Using Navier-Stokes Equations," J. Propulsion, 7(2), 231-239, (1991).
10. WANG, M. AND D. R. KASSOV, "A Perturbation Study of Acoustic Wave Propagation Through a Low Mach Number Shear Flow," Manuscript submitted to Journal of Fluid Mechanics, 1991a.
11. WANG, M. AND D. R. KASSOV, "Standing Acoustic Waves in a Low Mach Number Shear Flow," Manuscript submitted to AIAA Journal, 1991b.
12. WANG, M. AND D. R. KASSOV, "Transient acoustic processes in a low-Mach-number shear flow," J. Fluid Mech., 1992.
13. ZHAO, Q., Ph.D. Thesis, Department of Mechanical Engineering, University of Colorado at Boulder, 1994.

## 6. PERSONNEL

Graduate students

- Siming Mu
- Stephen Hevert

## 7. PUBLICATIONS

- Mu, S., and S. Mahalingam, "Numerical Simulation of Acoustic-Mean Flow Interaction," Bull. Am. Phys. Soc. II, (38) No. 12, p. 2218 (1993).
- Mu, S., and S. Mahalingam, "Direct Numerical Simulation of Acoustic-Mean Flow Interactions in 2D Ducts," accepted for publication in *AIAA Journal*, in press, (1995).

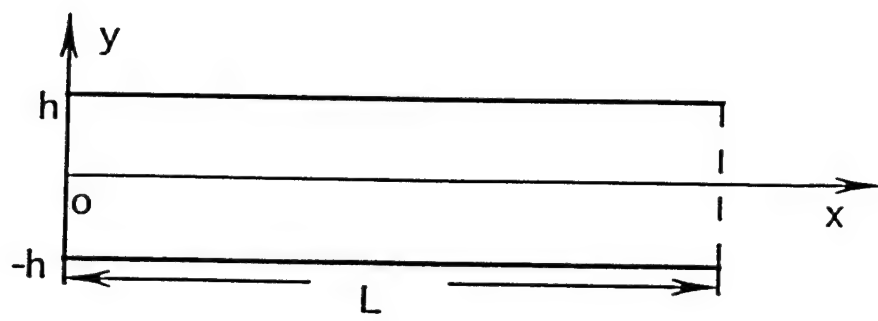


Figure 1 Schematic representation of computational domain and coordinate system definition.

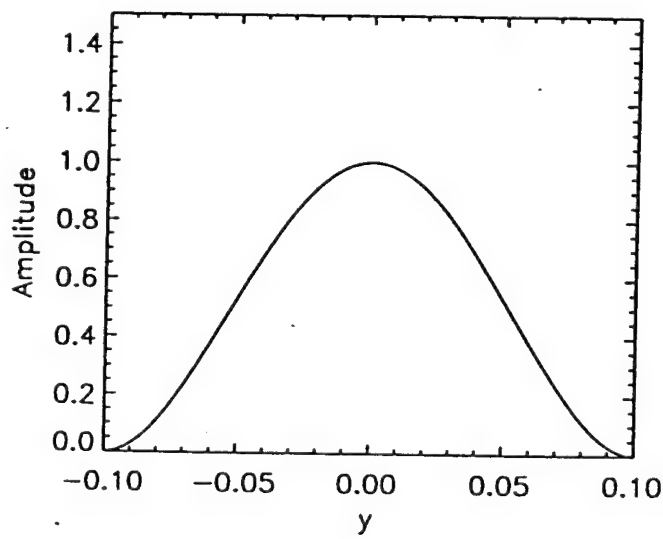
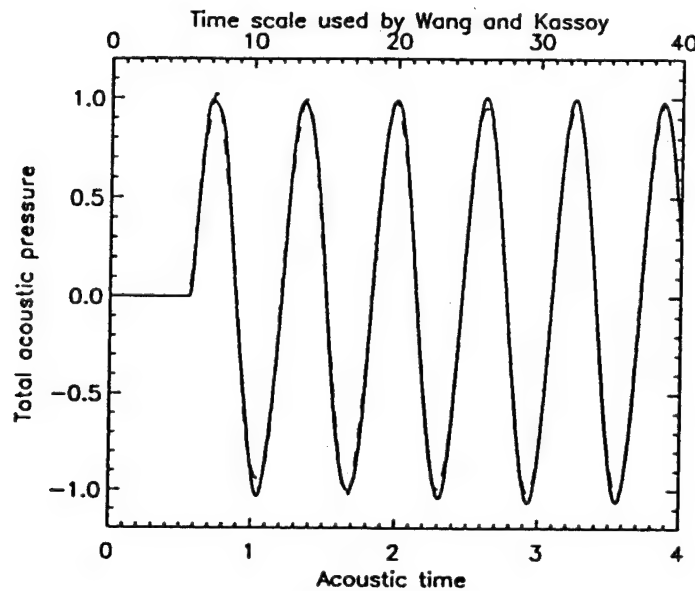


Figure 2 Profile of amplitudes of axial velocity disturbance used, normalized with respect to the centerline velocity for  $A = 1$ .

(a)



(b)

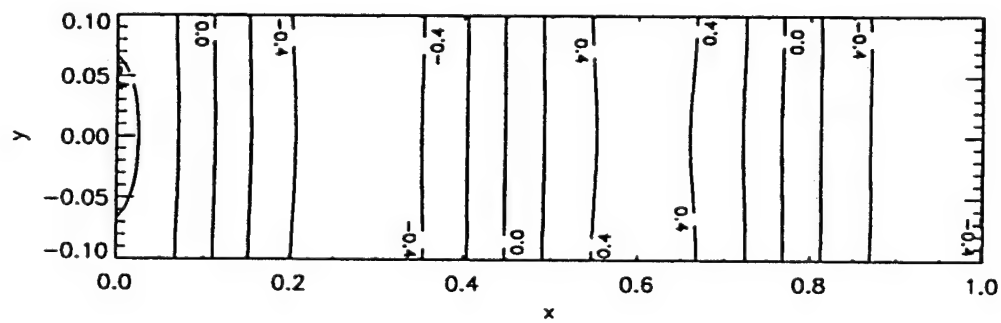


Figure 3 (a) Total acoustic pressure time history at  $x = 0.6$ , at wall (solid line) and center (dashed line); (b) total acoustic pressure contour at  $t = 3.25$  for  $\Omega = 10$ , mesh  $81 \times 81$  and acoustic  $Re = 20,000$ .

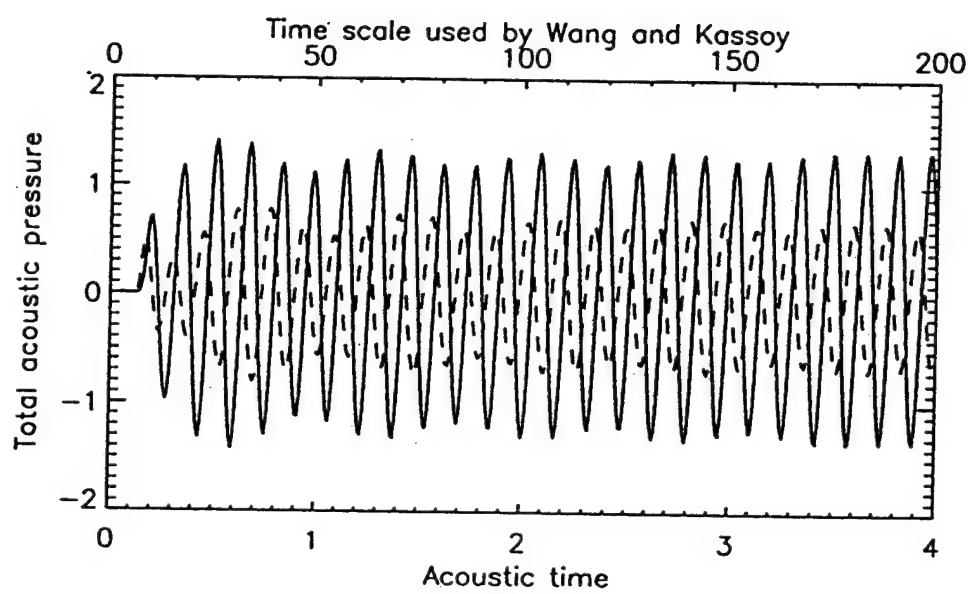


Figure 4 Total acoustic pressure time history at  $x = 0.15$ , center (dashed) and wall (solid) for  $\Omega = 40$ , mesh  $81 \times 81$  and acoustic  $Re = 20,000$ .

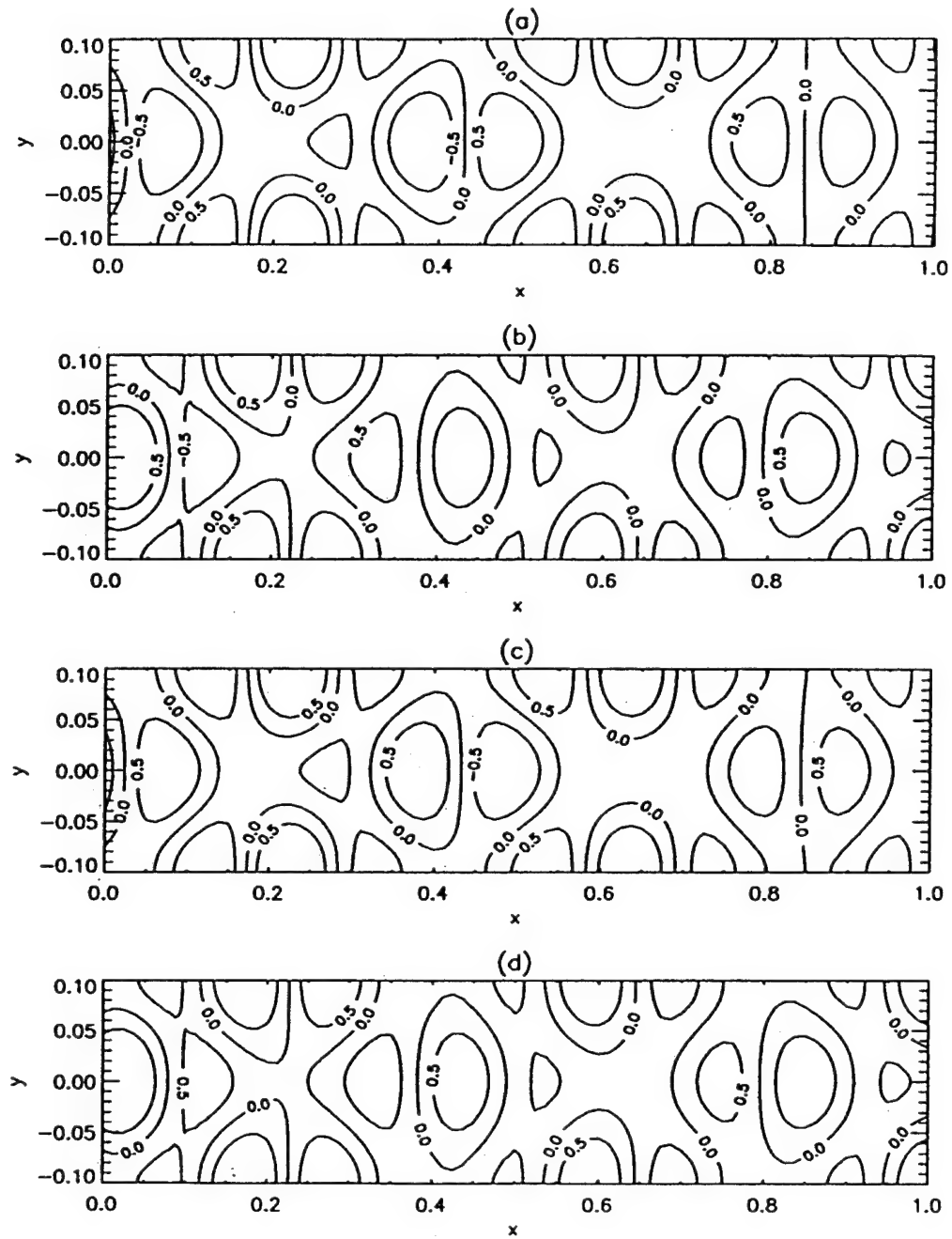


Figure 5 Total acoustic pressure contour at (a)  $t = 3.0$ , (b)  $t = 3.02$ , (c)  $t = 3.08$ , (d)  $t = 3.12$  for  $\Omega = 40$ , mesh  $81 \times 81$  and acoustic  $Re = 40$ .

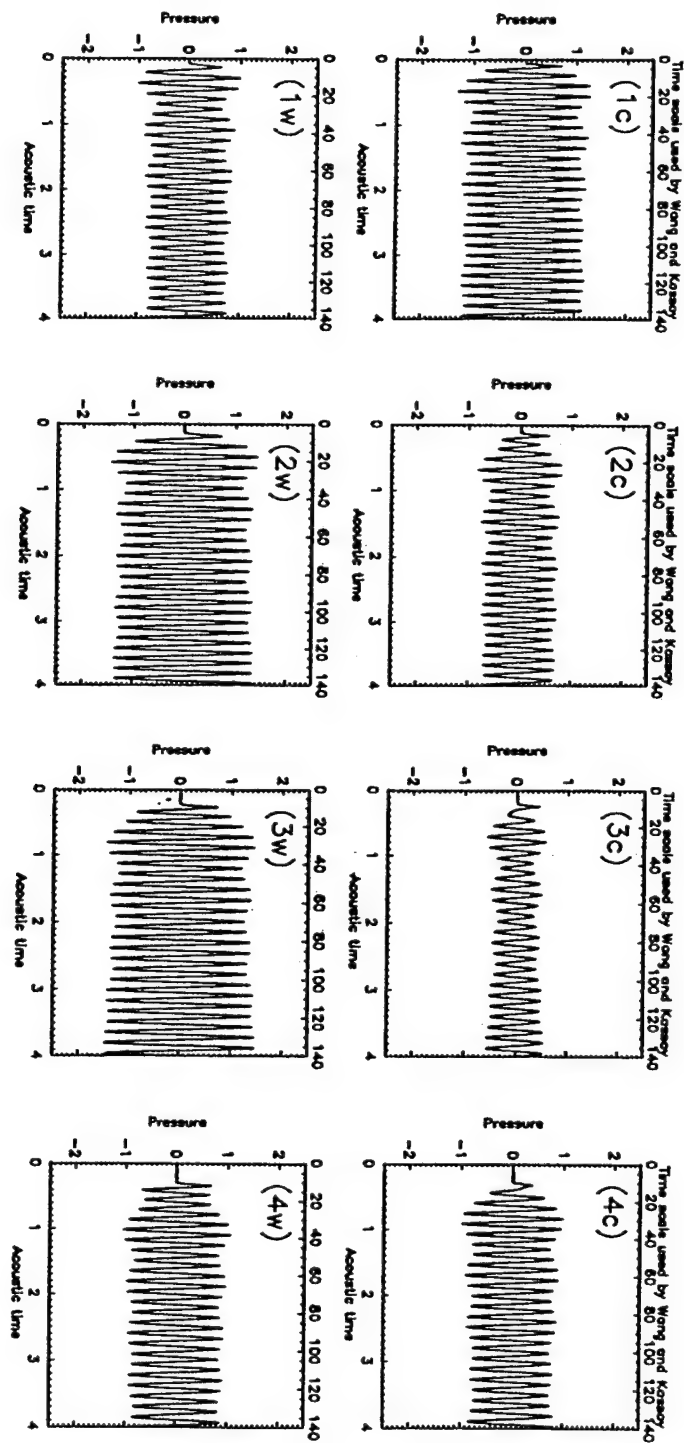


Figure 6 Total acoustic pressure time history at different locations. "c": centerline; "w": wall. (1) $x = 0.1$ , (2) $x = 0.2$ , (3) $x = 0.3$ , (4) $x = 0.4$  for  $\Omega = 40$ , mesh  $81 \times 81$  and acoustic  $Re = 20,000$ .

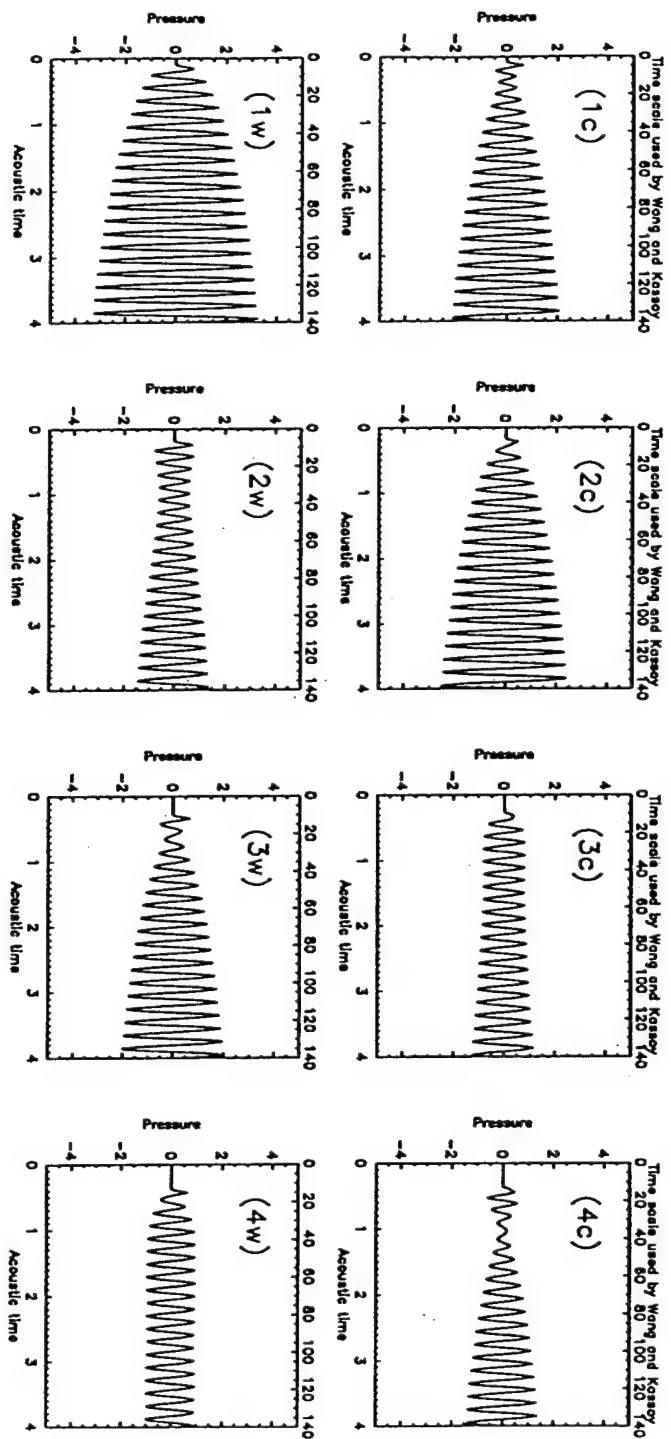


Figure 7 Total acoustic pressure time history at different locations. "c": centerline; "w": wall. (1) $x = 0.1$ , (2) $x = 0.2$ , (3) $x = 0.3$ , (4) $x = 0.4$  for  $\Omega = 10\pi$ , mesh  $81 \times 81$  and acoustic  $Re = 20,000$ .

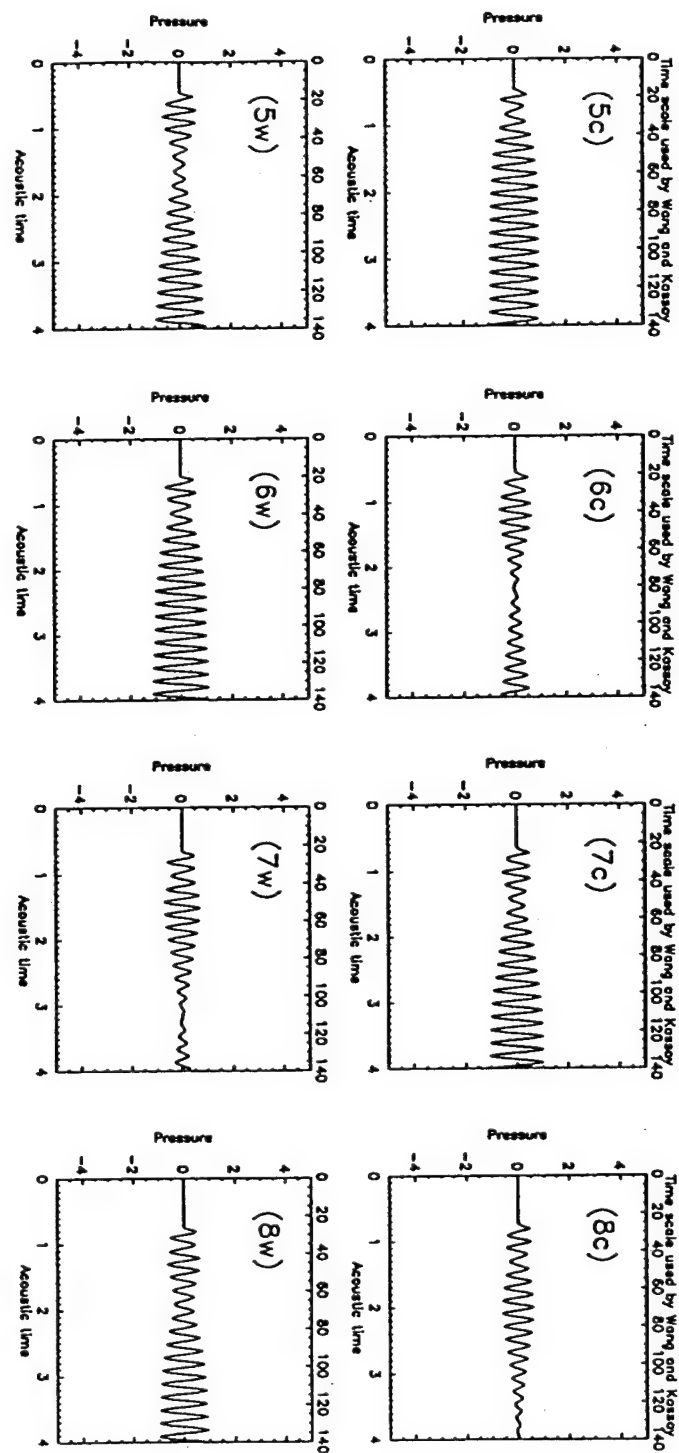


Figure 7 (Figure 7 Cont'd) Total acoustic pressure time history at different locations. "c": centerline; "w": wall. (5) $x = 0.5$ , (6) $x = 0.6$ , (7) $x = 0.7$ , (8) $x = 0.8$  for  $\Omega = 10\pi$ , mesh  $81 \times 81$  and acoustic  $Re = 20,000$ .

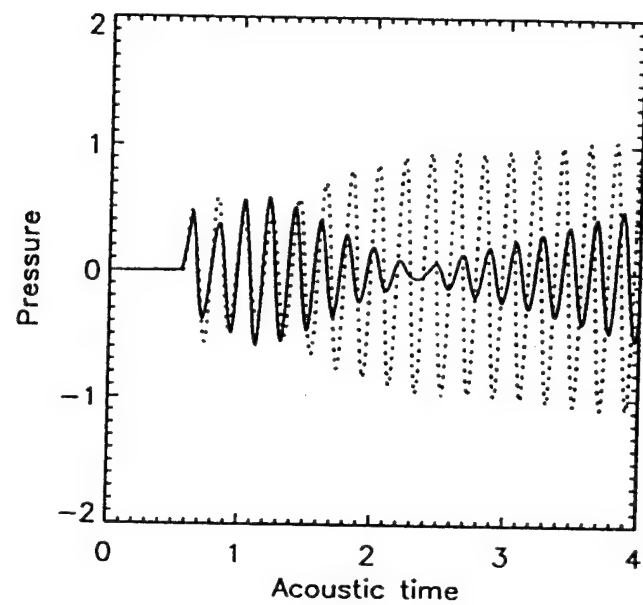


Figure 8 Overlay of pressure in Figure 7 (6c) and (6w).

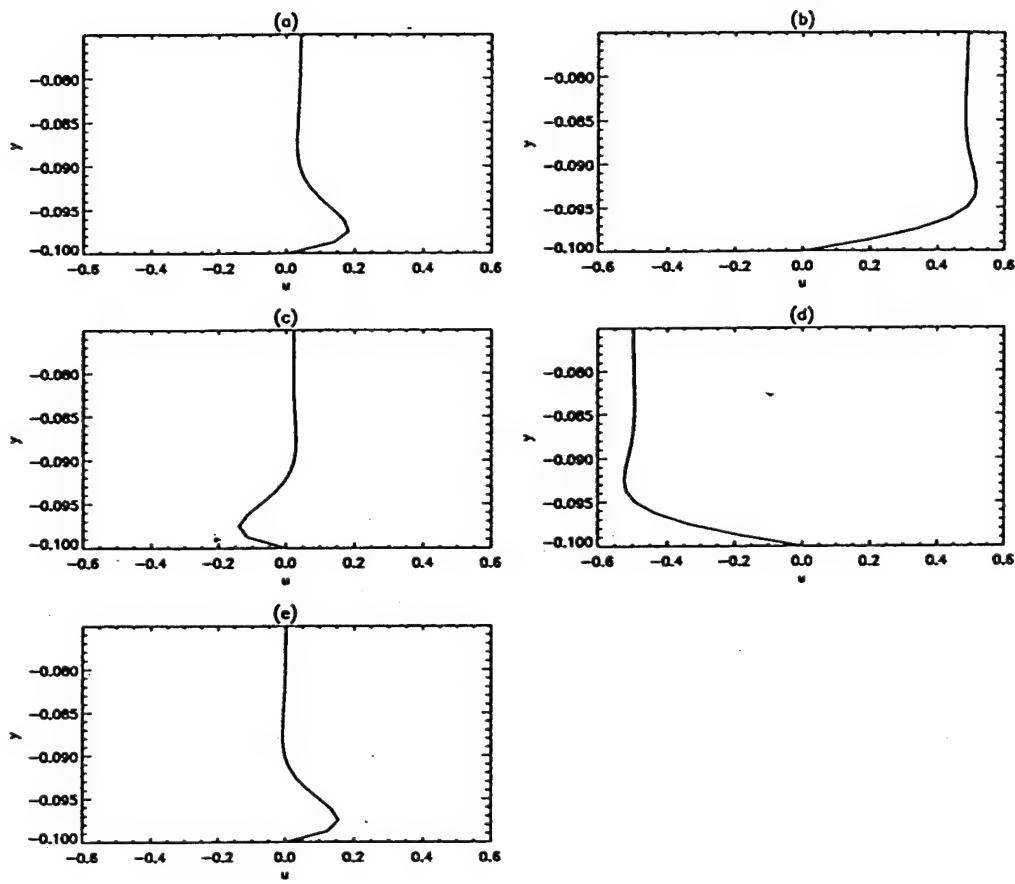


Figure 9 Axial acoustic velocity profiles at  $x = 0.5$  and (a)  $t = 3.0$ , (b)  $t = 3.14$ , (c)  $t = 3.30$ , (d)  $t = 3.45$ , (e)  $t = 3.45$  for  $\Omega = 10$ , mesh  $81 \times 161$  and acoustic  $Re = 20,000$ .

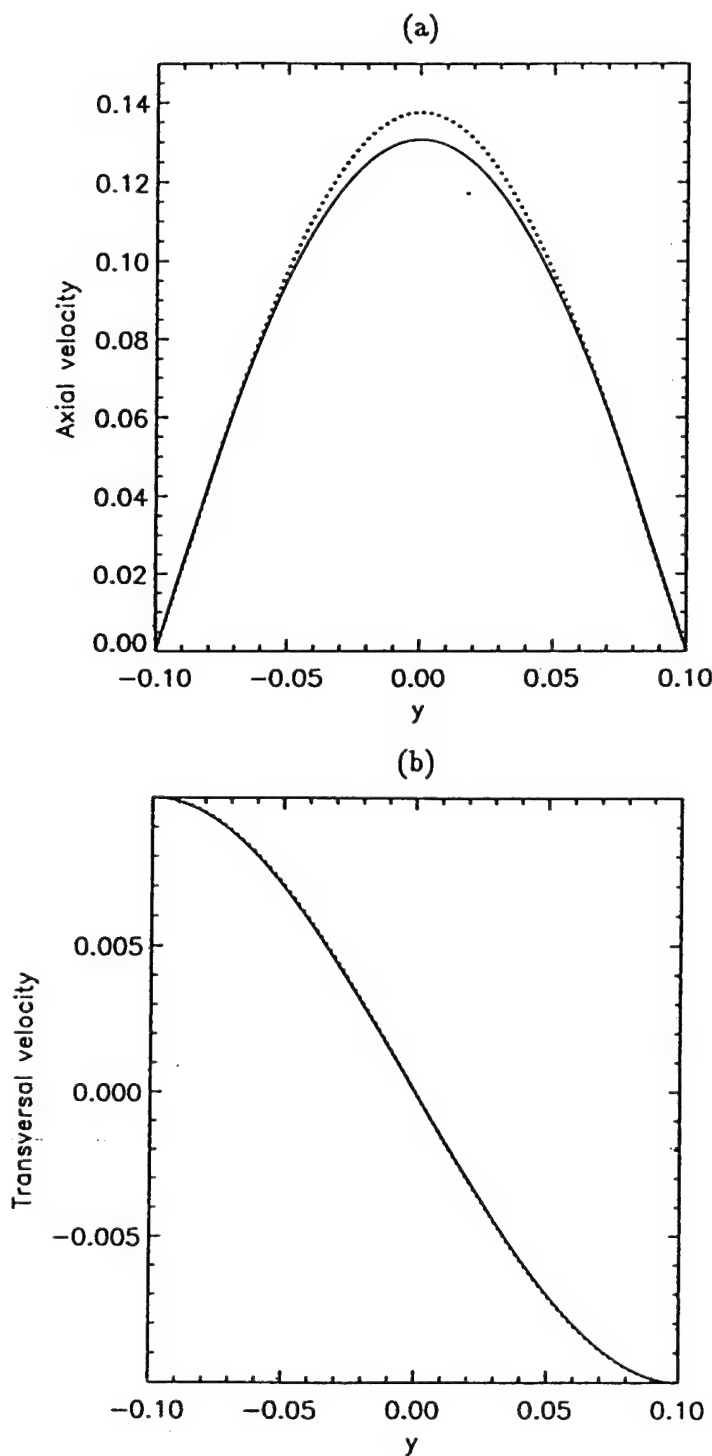


Figure 10 (a) Steady state axial velocity profiles at  $x = 0.5$  for acoustic  $Re = 20,000$  with side wall injection. Solid line: analytical solution, Dashed line: numerical solution; (b) Steady state transverse velocity profile.

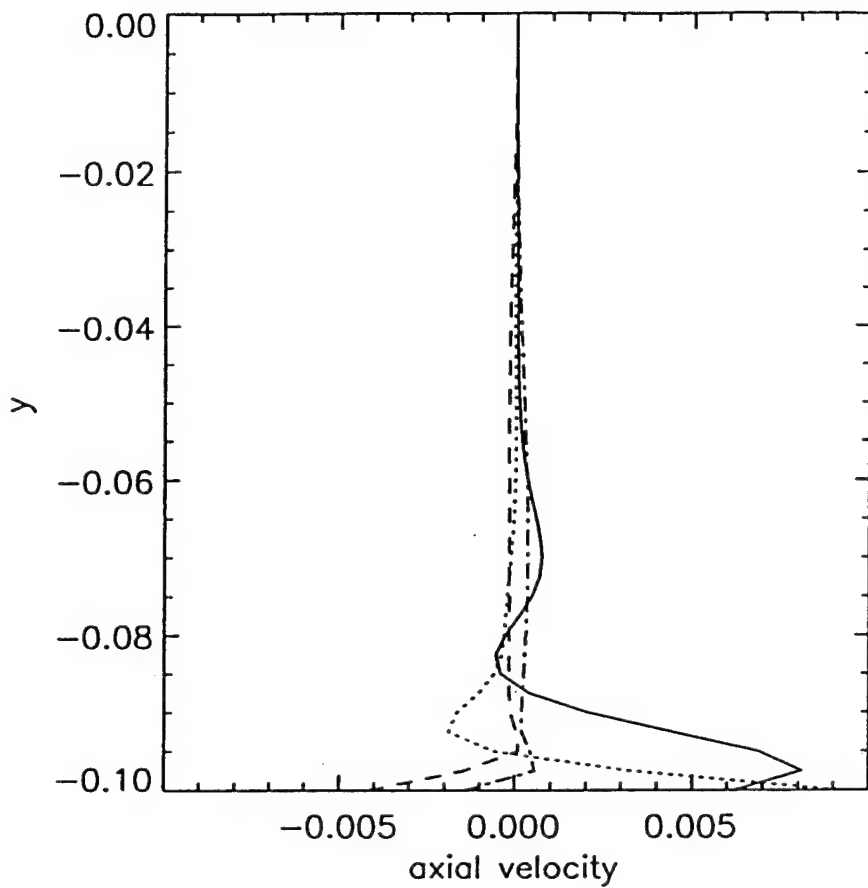


Figure 11 Profiles of the vortical component of the axial velocity at  $x = 0.5$  for acoustic  $Re = 20,000$  with side wall injection.  $\cdots \cdots : \Omega = 5,$   $\cdots \cdots \cdots : \Omega = 10,$   $\cdots \cdots \cdots \cdots : \Omega = 10\pi,$   $\text{—} : \Omega = 40$

## Direct Numerical Simulation of Acoustic-Shear Flow Interactions in Two Dimensional Ducts

Siming Mu<sup>1</sup>, and Shankar Mahalingam<sup>2</sup>

*Center for Combustion Research  
Department of Mechanical Engineering, University of Colorado  
Boulder, Colorado 80309-0427*

### Abstract

The interaction between an imposed monochromatic, time-dependent acoustic disturbance and a steady mean shear flow in a two-dimensional duct is studied using direct numerical simulation. Unlike previously reported numerical results, the long time acoustic response is captured through implementation of accurate non-reflecting boundary conditions. Below a certain cut-off frequency, the acoustic field is a nearly planar traveling wave propagating axially along the duct. Above this cut-off frequency, oblique waves are generated due to both acoustic refraction and cross-stream dependent source oscillation, leading to an alternating pattern of higher acoustic pressures at the wall and the centerline, downstream of the disturbance source. At resonant conditions, the growth of the oblique wave, which is nearly transverse, dominates the axial wave, leading to a phase change of 180 degrees after their interaction. The thickness of the acoustic boundary layer and its response to imposed disturbances are also in good agreement with theory. These results are consistent with previously published theoretical predictions, and represent their first numerical verification.

---

<sup>1</sup>Graduate Student, Department of Mechanical Engineering, University of Colorado, Boulder, CO-80309-0427

<sup>2</sup>Assistant Professor, Department of Mechanical Engineering, University of Colorado, Boulder, CO-80309-0427, Member AIAA, and corresponding author

## Nomenclature

$a_\infty$	reference speed of sound, also reference velocity
$C_p$	constant pressure specific heat, temperature independent
$e_t$	internal energy per unit volume
$h$	duct half-width
$i, j, k$	denote coordinate directions in Cartesian tensor notation
$L$	computational length of duct
$M$	mean flow Mach number
$p$	pressure
$Pr$	Prandtl number
$q_j$	heat flux vector component in the $j$ -th direction
$Re$	acoustic Reynolds number in the calculation
$Re_c$	duct Reynolds number
$T$	temperature
$t$	time variable
$u_k$	velocity component in the $k$ -th coordinate direction
$\hat{u}$	axial acoustic velocity disturbance
$v$	velocity component in the $y$ coordinate direction
$x, y$	spatial variables along the $x$ and $y$ coordinate directions
$x_j$	independent spatial variable along the $j$ -th coordinate direction

## Greek symbols

$\alpha$	computational duct aspect ratio
$\gamma$	constant specific heat ratio
$\delta$	acoustic boundary layer thickness
$\epsilon$	small parameter used in perturbation analysis
$\kappa$	viscosity power law exponent
$\mu$	coefficient of dynamic viscosity
$\nu$	coefficient of kinematic viscosity
$\Omega$	dimensionless frequency of imposed oscillation
$\tau_{ij}$	stress tensor

## Subscripts and superscripts

'	denotes dimensional quantity
$\infty$	denotes reference quantity, chosen at stagnant conditions
$\sim$	denotes acoustic disturbance
$s$	undisturbed steady state

## Introduction

The interaction of an acoustic wave disturbance with a shear flow provides a mechanism for transfer of energy between the mean, and various modes of the acoustic flow. This problem is significant as it provides a vital link in the chain of events that could lead to combustion-driven acoustic instability in solid rocket motors. However, in practical motors, the various

mechanisms that contribute to amplification and damping of acoustic energy are intimately related to the acoustic mode, and the type of propellant lining the motor surface.<sup>1</sup> This makes it difficult to isolate physical mechanisms associated with individual processes when the full problem is investigated. Thus, the focus of this paper is on the mechanism of energy exchange between the mean and various modes of the acoustic flow in a sufficiently simplified flow situation for which theoretical results are available. This problem is investigated via Direct Numerical Simulation (henceforth, DNS) of the interaction between an imposed acoustic velocity disturbance in an otherwise steady shear flow established in a two-dimensional duct. In DNS, the complete time-dependent system of equations is solved without any explicit modeling, such as turbulence modeling. This procedure has been successfully applied to a variety of incompressible, compressible, and reacting flows.<sup>2</sup>

Much of past analytical work has focused on obtaining quasi-steady solutions to a linearized wave equation describing acoustic wave propagation in a fully developed duct flow.<sup>3</sup> Using this as a basis, both downstream propagating<sup>3</sup> and upstream propagating acoustic waves<sup>4,5</sup> have been investigated. Results suggest that in the former case, the acoustic pressure at the wall is larger than that at the centerline; the reverse is true in the latter case. Since this method presumes the form of the solution, it cannot predict the evolution from an initial disturbance to the quasi-steady form. Baum and Levine<sup>6</sup>, and subsequently, Wang and Kassoy<sup>7</sup> proceeded to rectify this shortcoming by investigating an initial-boundary value problem *albeit* using entirely different approaches. Baum and Levine solved the compressible Navier-Stokes equations numerically for a Reynolds number, based on centerline velocity and duct width, of approximately  $10^5$ . A turbulence model was included in their calculations. A disturbance was introduced at a certain cross section and its evolution was tracked. They found that acoustic refraction effects increased with the frequency of the imposed disturbance. The relationship between the wall and centerline acoustic pressure for upstream and downstream propagation of acoustic waves, in a qualitative sense, was consistent with that predicted by the quasi-steady theory.<sup>4,5</sup> At the outflow boundary, they had difficulty in prescribing non-reflecting conditions, and hence they terminated their computations when the imposed wave reached the downstream boundary of their computational domain. Thus the long-time transient solution, which has since been demonstrated to be extremely important<sup>7</sup> was not available in their work. This may also be the reason why they did not observe oblique waves and resonant mode oscillations. Using a rational perturbation procedure, Wang and Kassoy<sup>7</sup> solved an initial-boundary value problem to describe acoustic processes in a two-dimensional shear flow in a duct for small mean flow Mach number and large Reynolds number. Their results indicate that as a result of leading order axial wave refraction by the shear flow, oblique propagating waves develop. This refraction effect increases with the driving frequency of the imposed acoustic disturbance and the mean flow Mach number. The oblique waves evolve into purely amplifying transverse waves at frequencies corresponding to resonance. The initial-boundary value approach discussed above differs from what may be termed a normal mode analysis that is often applied to problems involving combustion-driven acoustic instability in solid rocket motors<sup>8,9,10</sup> and pulsed combustors.<sup>11</sup> In the traditional approach,<sup>8,9,10</sup> the amplitudes of either the classical acoustic modes or modes suitably mod-

ified to account for processes that influence the basic acoustic modes are described via an infinite system of coupled ordinary differential equations. The idea is then to obtain conditions that could lead to growth or amplification of different modes, and also to predict conditions that could lead to limit-cycle type behavior.

The objective in the present paper is to verify the existence of, and to understand the role of oblique waves generated through acoustic refraction when a monochromatic, acoustic velocity disturbance introduced at a fixed duct location is allowed to interact with a steady shear flow in a two-dimensional duct. In particular, we seek to validate the analytical results obtained by Wang and Kassoy<sup>7</sup> and use their predictions to examine and interpret the complex acoustic structure that is obtained. The approach adopted is an accurate solution to the compressible Navier-Stokes equations through DNS of the problem.

### Problem Formulation

The full compressible two-dimensional Navier-Stokes equations are solved as an initial value problem using a code originally developed by Baum and Poinsot<sup>12</sup> for reacting flows and adapted for the present research. The computational domain and coordinate system are represented in Fig. 1. The equations are rendered dimensionless using the duct length  $L$ , speed of sound at stagnant conditions  $a_\infty$ , the corresponding density  $\rho_\infty$ , and the dynamic pressure  $\rho_\infty a_\infty^2$ . The reference temperature is  $(\gamma - 1)T_\infty$ . The reference viscosity used is  $\mu_\infty = \mu(T_\infty)$ . The reference time is thus the acoustic time  $L/a_\infty$ . The dimensionless parameters governing the problem are the Reynolds number defined as

$$Re = \frac{\rho_\infty a_\infty L}{\mu_\infty}, \quad (1)$$

and the Prandtl number  $Pr = \mu_\infty C_p / \lambda_\infty$ , where  $\lambda_\infty = \lambda(T_\infty)$ . Note that the duct aspect ratio defined as

$$\alpha = \frac{L}{2h}, \quad (2)$$

although not a parameter, appears in the analysis since the computational domain is finite. By applying non-reflecting boundary conditions as discussed in the next section, the flow field in a duct of infinite length is effectively simulated. Henceforth all quantities are dimensionless. Dimensional quantities where appropriate are indicated by a prime. The dimensionless form of the governing equations written in Cartesian tensor notation appears below:  
Continuity,

$$\frac{\partial \rho}{\partial t} + \frac{\partial \rho u_j}{\partial x_j} = 0, \quad (3)$$

momentum,

$$\frac{\partial \rho u_i}{\partial t} + \frac{\partial \rho u_i u_j}{\partial x_j} = -\frac{\partial p}{\partial x_i} + \frac{1}{Re} \frac{\partial \tau_{ij}}{\partial x_j}, \quad (4)$$

and energy,

$$\frac{\partial \rho e_t}{\partial t} + \frac{\partial (\rho e_t + p) u_j}{\partial x_j} = \frac{1}{Re} \frac{\partial (u_i \tau_{ij})}{\partial x_j} - \frac{1}{Re Pr} \frac{\partial q_j}{\partial x_j}. \quad (5)$$

The internal energy per unit volume is given by

$$e_t = \frac{1}{2} \rho u_k u_k + \frac{p}{\gamma - 1}. \quad (6)$$

The stress tensor  $\tau_{ij}$  and the heat flux vector  $q_j$  are taken for a Newtonian fluid with the Fourier model for heat conduction as follows:

$$\tau_{ij} = \mu \left( \frac{\partial u_i}{\partial x_j} + \frac{\partial u_j}{\partial x_i} - \frac{2}{3} \delta_{ij} \frac{\partial u_k}{\partial x_k} \right), \quad q_i = -\lambda \frac{\partial T}{\partial x_i} \quad (7)$$

The dynamic viscosity  $\mu$  is dependent on temperature such that  $\mu \sim T^\kappa$ , where the exponent  $\kappa$  is a constant. The thermal conductivity  $\lambda$  is related to the dynamic viscosity through the constant Prandtl number. The equation of state is

$$p = \rho T \frac{\gamma - 1}{\gamma}. \quad (8)$$

### Numerical Method and Boundary Treatment

A compact sixth-order accurate finite difference scheme developed by Lele<sup>13</sup> is used to approximate the first and second derivatives in the governing equations. The order of accuracy is fourth and third respectively at points adjacent to, and on the boundary of the computational domain. This scheme requires solution of a tridiagonal matrix in order to compute the derivatives. The advantage of the compact scheme over more familiar finite-difference schemes is that it provides spectral-like resolution of both the amplitude and phase of the solution, thereby enabling the scheme to accurately capture acoustic wave behavior. A complete analysis of this scheme including a comparison of dispersion errors with traditional finite difference schemes is presented by Lele.<sup>13</sup> A third-order explicit Runge-Kutta scheme is adopted for time-advancement of the semi-discrete equations.

One critical requirement for capturing the wave characteristics of the acoustic field is accurate treatment of boundary conditions. In the present paper, a systematic boundary treatment method, namely Navier-Stokes Characteristic Boundary Condition (NSCBC), is utilized.<sup>14</sup> Based on the idea of characteristics for Euler equations<sup>15</sup> the NSCBC assumes that the waves propagated by Navier-Stokes equations are associated with only the hyperbolic part of the equation.<sup>14</sup> Thus the first derivative normal to a boundary appearing in the convective term of the Navier-Stokes equations may be rewritten in terms of the amplitude variations of the characteristic waves represented by Navier-Stokes equations. For those characteristic waves propagating out of the domain, the values of their amplitude variation are completely defined by data from within the computational domain through use of one-sided approximations. Numerical stability is achieved since this amounts to upwind differencing. For those waves propagating into the computational domain, boundary conditions are needed to specify the values of their amplitude variations. There is no exact method to compute the amplitude variations of these incoming waves. A set of locally one-dimensional inviscid (LODI) equations are used to infer the values of the incoming amplitude variations from the boundary conditions. Derivatives parallel to the boundary pose no problems and are treated exactly as in the interior. The treatment of viscous conditions is based on the method suggested in Ref. 14. These terms go to zero as the viscosity goes to zero. For a detailed discussion of the NSCBC procedure, the paper by Poinsot and Lele<sup>14</sup> may be consulted.

In this paper the flow considered is subsonic with a mean flow Mach number  $M \approx 0.08$ . Unless otherwise noted,  $\alpha = 5$ ,  $Re = 20000$ , and  $Pr = 1$ . Thus the Reynolds number based on the mean flow velocity and duct width,  $Re_c = M Re / \alpha = 320$ .

Reflecting boundary conditions are used at the inlet. The transverse velocity component  $v$  is set to zero, the axial velocity profile  $u = u(0, y, t)$ , such that  $u(0, -1/2\alpha, t) = u(0, +1/2\alpha, t) = 0$ , is prescribed, and a constant inlet temperature,  $T(0, y, t) = 1/(\gamma - 1)$  is prescribed. At the lateral boundary, no-slip velocity and isothermal conditions are prescribed. At the outflow, non-reflecting boundary conditions based on the method developed in Ref. 14 are imposed. This allows acoustic waves to propagate out of the domain with little or no reflections, and thus enables us to carry out long-time stable computations. A steady flow is established by initializing the domain with stagnant flow, and raising the pressure at the inlet by 5% of the initial uniform pressure,  $p = 1$ . This steady state flow field is used as initial conditions for several transient problems in which a time-dependent perturbation is imposed on the incoming streamwise velocity.

## Results and Discussion

### Code Validation

Several test problems were simulated to verify that the code and boundary condition treatment are satisfactory. Both non-reflecting and reflecting boundary conditions were examined.<sup>16</sup> In order to test the NSCBC procedure, a very viscous test problem<sup>14</sup> was simulated. The inlet conditions imposed are

$$u(0, y, t) = u_0 \cos^2(\pi y \alpha), \quad v(0, y, t) = 0, \quad T(0, y, t) = T_0, \quad (9)$$

where  $u_0$ ,  $T_0$  are constants. Non-reflecting conditions are imposed at the outlet. The Reynolds number  $Re = 2000$  and a uniform  $41 \times 41$  mesh was used. Steady state contour plots of  $u/u_0$ ,  $100(p - p_\infty)/p_\infty$ , and  $100(T - T_\infty)/T_\infty$  are virtually identical to past numerical<sup>14</sup> and analytical results,<sup>14</sup> thereby validating the code and boundary conditions. For the sake of brevity, in Fig. 2, only contour plots of temperature are presented. Transient results presented in the remainder of this section were obtained on a uniform  $81 \times 81$  mesh. Grid independence was verified by repeating the calculations on a  $161 \times 161$  grid. All calculations were performed on a Cray C-90 at the San Diego Supercomputing Center.

### Nature of imposed disturbance

A transient acoustic field is generated by imposing a single frequency disturbance on the inlet axial velocity. No slip at the lateral walls demands that the amplitude of the disturbance be zero at  $y = \pm 1/2\alpha$ . Although the analysis in Ref. 7 is quite general, the results they present are for constant amplitude and linear variation of amplitude and thus our results can only be qualitatively related to their theoretical results. The axial velocity disturbance  $\hat{u}(y, t)$  was chosen to have the following mathematical form

$$\hat{u}(y, t) = AU(y) \sin \left[ \alpha\pi \left( y + \frac{1}{2\alpha} \right) \right] \sin \Omega t \quad (10)$$

where  $\Omega$  is the dimensionless frequency defined through  $\Omega = \Omega' L/a_\infty$ , and  $U(y)$  is the initial, steady axial velocity at the inlet. The quantity  $A$  is a constant that controls the magnitude of the disturbance. The disturbance is introduced by specifying an axial inlet velocity profile of the form

$$u(0, y, t) = U(y) + \epsilon \hat{u}(y, t) \quad (11)$$

The quantity  $\epsilon$  is the small parameter introduced in Ref. 7. By performing a Fast Fourier Transform (FFT) in  $y$  on the discrete version of Eq. (10), it is found that the primary transverse mode components are the zeroth and first modes, with higher mode amplitudes being less than 2% of these. Thus it is reasonable to expect that the simulation results will compare well with Ref. 7, at least qualitatively.

Theory<sup>7</sup> for  $y$ -independent amplitude function suggests that for  $\Omega < \alpha n\pi$ ,  $n = 1, 2, 3, \dots$ , only axial waves would exist. When  $\Omega > \alpha n\pi$ , refraction-induced oblique waves begin to appear. In the present simulation  $\alpha = 5$ , and since the mean flow is symmetric with respect to the duct center plane, only even values of  $n$  are relevant. This leads to the first cut-off frequency of  $10\pi$  (corresponding to  $n = 2$ ) above which oblique waves are expected to be generated. The leading order solution is uninfluenced by the mean flow except through a bulk convection effect. Through an examination of the second-order acoustic solution Wang and Kassoy<sup>7</sup> predicted that  $\Omega = \alpha n\pi$  corresponds to resonant conditions. Classical quasi-steady theory<sup>3</sup> cannot describe resonant oscillations, and previous numerical simulations were unable

to capture this phenomenon due to difficulties in implementing outflow boundary conditions.<sup>6</sup> The numerical solutions were curtailed when the disturbance reached the outflow boundary, and hence the long-time behavior, required to observe resonant effects, was not studied.<sup>6,7</sup> In the present work, several frequencies were examined. In the following sub-sections, results are presented for different values of  $\Omega$  that were chosen to represent typical characteristics of different frequency regimes. Since the no-slip wall condition in the simulations demands that the perturbation amplitude be  $y$ -dependent, it is important to recognize that higher modes (non-planar) are expected to be generated directly by the source, in addition to refraction of the planar component.<sup>7</sup> Using the decomposition in Ref. 7, the total acoustic pressure  $\hat{p}$  and axial acoustic velocity  $\hat{u}$  were obtained as

$$\hat{p} = \frac{1}{\gamma M \epsilon} [p(x, y, t) - p_s(x, y)], \quad \hat{u} = \frac{1}{\epsilon} [u(x, y, t) - u_s(x, y)] \quad (12)$$

where  $p_s$ , and  $u_s$  are the undisturbed steady pressure and axial velocity respectively. In all cases, computations were carried out up to four acoustic time units, with  $\epsilon = 0.1$ .

#### Acoustic Pressure Field for $\Omega = 10$

The frequency  $\Omega = 10$  is below the first “cut-off” frequency of  $10\pi$ . Fig. 3 represents the total acoustic pressure time history at  $x = 0.6$ . For convenience, the time scale used by Wang and Kassoy<sup>7</sup>

$$t_w = t' \Omega' \quad (13)$$

where  $t'$  is the dimensional time is also shown in Fig. 3. The amplitude of acoustic pressure at the centerline is slightly smaller than that at the wall (also true at other  $x$  locations) due to refraction of the downstream propagating acoustic wave. An examination of acoustic pressure contours suggests that sufficiently far downstream from the inlet, the waves are nearly planar. Thus no oblique waves appear for the conditions of the simulation. This result is in qualitative agreement with analytical prediction.<sup>7</sup> An FFT analysis of the acoustic pressure with respect to  $y$  at various axial locations and times (see Fig. 4) shows a dramatic decay in amplitudes of the first transversal spatial component while very little decay in amplitudes is seen for the zeroth component. Since the latter corresponds to the planar part of the disturbance, this result is consistent with the earlier remark that at locations sufficiently far downstream from the disturbance source, only the planar component survives.

#### Acoustic Pressure Field for $\Omega = 40$

The forcing frequency  $\Omega = 40$  is just above the first cut-off frequency. The acoustic pressure time history at fixed locations is presented in Fig. 5. A comparison of Fig. 5 with Fig. 3 reveals several interesting features. At early times, after the first arrival of the waves, an increase

in amplitude can be observed. Then the amplitudes themselves begin to oscillate although at a much reduced frequency. Recall from Ref. 7 that a plane wave (zeroth transversal spatial mode) with its frequency above the cut-off frequency generates oblique waves as it travels downstream. In the present work, the acoustic source is non-planar due to the  $y$ -dependent amplitude function, and thus oblique waves are expected to be excited, in addition to refraction of the axial mode giving rise to oblique waves. The result of these two processes is a variation in amplitudes of acoustic pressure as depicted in Fig. 5. Further it is evident from Fig. 5 that the pressure amplitude for  $\Omega = 40$  is greatly enhanced compared to that for  $\Omega = 10$  (see Fig. 3). This enhancement arises from the increased amplitudes of the first transversal spatial mode as can be seen from Figs. 6(a-b). From these plots it is apparent that the amplitudes of the first transversal spatial mode grow to values having the same order as those of the zeroth mode while the amplitudes of the zeroth mode varies very little compared to those for  $\Omega = 10$ .

### Acoustic Pressure Field for $\Omega = 10\pi$

The angular frequency  $\Omega = 10\pi$  corresponds to the second resonant mode. Figure 7 depicts the acoustic pressure time history at the wall and centerline at different axial locations. The general feature of resonant oscillation is displayed at locations (1c) and (1w) (here w and c denote wall and centerline respectively), where the acoustic pressure amplitudes increases consistently with time. However, axial stations 2 and 3 display slightly different features. One can see that at some axial locations (stations 2w, 3w, and 4c) the signal initially decreases and subsequently increases. This behavior is very similar to that reported by Wang and Kassoy.<sup>7</sup> Although Wang and Kassoy<sup>7</sup> focus their discussion on second order acoustic pressure, their qualitative description is also valid for the total acoustic pressure because the first order acoustic pressure is just a plane sine wave propagating axially, for  $y$ -independent source amplitude. The acoustic pressure amplitude at different axial stations increases with time after sufficient time elapses. However, the amplitude of acoustic pressure may initially decrease with time "owing to destructive interference".<sup>7</sup> Previous numerical investigation by Baum and Levine<sup>6</sup> was limited to very short time solution due to difficulties alluded to earlier. Both the present numerical and previous analytical results show that an examination of the short-time solution is insufficient to conclude whether resonant amplifications are occurring.

Acoustic pressure data at downstream locations (stations 4 through 8 in Fig. 7) reveals some additional features that have not been reported previously. After the initial decrease in amplitude due to "destructive interference" the amplitudes at all locations start to increase with time. Then at some locations wave amplitudes quickly stop amplifying and remain nearly constant, suggesting that extraction of acoustic energy (to the mean), and viscous dissipation are occurring. On the other hand, at other locations amplitudes start to decrease again and eventually reach a value close to zero. When the acoustic pressure amplitudes increase once again, they have undergone a phase change of  $\pi$  with respect to the phase of the signal at early time. This can be seen by overlaying the data from locations (6c) and (6w) of Fig. 7, not included here for the sake of brevity. This behavior of acoustic pressure waves suggests an interaction between an axially traveling wave and another much stronger

wave which arrives after the axial wave, and has an opposite phase with respect to the axial wave. Based on theoretical results<sup>7</sup> it may be concluded that the alternating appearance of this behavior under resonant conditions is caused by the interaction of axial with nearly transverse waves. Unlike the  $\Omega = 40$  case, transverse waves for  $\Omega = 10\pi$  are excited and grow with time due to resonance. A pictorial representation of the instantaneous acoustic pressure fields is presented in Figs. 8(a-d). The direction along which the pressure gradient is a maximum is indicative of the instantaneous wave structure as a result of axial and transverse mode interaction. Based on a comparison of the present results with theory<sup>7</sup>, the following observations may be made:

1. Present simulation shows that under resonant conditions, significant interaction between the nearly transverse and axial waves only appears downstream, sufficiently far away from the disturbance source probably because the waves need a certain amount of travel distance and time to collect sufficient acoustic energy and settle into nearly transverse waves.
2. From the analysis presented in Ref. 7, where the source amplitude function is  $y$ -dependent, it is evident that the magnitude of the higher modes is of the same order as the axial mode and the effect of refraction of the axial mode is of lower order. This suggests that the present results are dominated by the source structure.

### **Acoustic Boundary Layer**

The existence of an acoustic boundary layer is another interesting feature that arises naturally due to the acoustic-mean flow interaction. It is a region close to the wall within which an overshoot of axial acoustic velocity can be observed as depicted in Fig. 9. The magnitude of the overshoot reaches a maximum value whenever the axial acoustic velocity in the core changes sign. This phenomenon is attributable to the Richardson's annular effect.<sup>6,7</sup> The thickness of the acoustic boundary layer  $\delta$ , is given in Ref. 7 by

$$\delta = 5 \left[ \frac{M}{\gamma Re_c} \right]^{\frac{1}{2}} \quad (14)$$

This thickness, expressed as a fraction of the duct width, is defined as the distance from the wall where the axial velocity reaches 97.3% of the core value. Approximately eight grid points are present within this boundary layer, a value that is sufficient to resolve the acoustic boundary layer. In the present case,  $\delta = 5.6\%$  is the predicted value. Numerical solution in Figs. 9(a-d) gives a thickness of 5.0 to 5.5% which is good agreement with analytical prediction.

### **Summary and Conclusions**

In the present paper, direct numerical simulation was performed to study the effect of an acoustic disturbance source in the presence of a mean shear flow in a two-dimensional duct.

Results show good agreement with analytical predictions of Wang and Kassoy.<sup>7</sup> Several interesting features associated with this problem have been observed.

1. There exists a critical frequency, above which oblique waves are generated. The interaction between oblique waves and axially traveling waves results in variation of amplitudes of acoustic pressure.
2. Amplified oblique waves that are nearly transverse due to resonant disturbances are observed for the first time. The rate of amplification of these waves is much higher than that of the axially traveling waves. At certain locations of the domain, this strong nearly transverse wave interacts with the axial wave, causing a dramatic change in both wave amplitude and phase.
3. For resonant disturbances with several transversal spatial modes, the growth rate varies significantly for different modes, being the highest for the first transverse mode.
4. The present simulation resolved the acoustic boundary layer very well. The thickness estimated through numerical simulation is in agreement with that predicted by theory.

#### Acknowledgments

The research presented in this paper is sponsored by the Air Force Office Of Scientific Research through grant AFOSR F-49620-92-J045, and monitored by Dr. Mitat Birkan. The authors acknowledge computer support on the Cray C-90 provided by the San Diego Supercomputing Center. The authors are grateful to M. Baum, and T. J. Poinsot for permitting us to use their 2D code in the present study. Fruitful discussions with D. R. Kassoy is gratefully acknowledged. The authors express their thanks to an anonymous referee that highlighted the significance of the cross-stream position dependent acoustic source function.

## REFERENCES

1. Price, E. W., "Experimental Observations of Combustion Instability", *Progress in Astronautics and Aeronautics*, Eds. K. K. Kuo, and M. Summerfield, Vol. 90, 1978, pp. 733-790
2. Givi, P., "Model-free Simulations of Turbulent Reactive Flows," *Prog. Energy Combust. Sci.*, Vol. 15 (1), 1989.
3. Pridmore-Brown, D. C., "Sound Propagation in a Fluid Flowing Through an Attenuating Duct", *J. Fluid Mech.*, Vol. 4, 1958, pp. 393-406.
4. Munger, P., and G. M. Gladwell, "Acoustic Wave Propagation in a Sheared Flow Contained in a Duct", *J. Sound Vib.*, Vol. 9, 1969, pp. 28-48.
5. Hersh, A. S., and I. Catton, "Effect of Shear Flow on Sound Propagation in Rectangular Ducts", *J. Acoustic Society of America*, Vol. 50, No. 3, 1971, pp. 992-1003.
6. Baum, J. D., and J. N. Levine, "Numerical Investigation of Acoustic Refraction", *AIAA Journal*, Vol. 25, No. 12, 1987, pp. 1577-1586.
7. Wang, M., and Kassoy, D. R., "Transient Acoustic Processes in a Low-Mach Number Shear Flow", *J. Fluid Mech.*, Vol. 238, 1992, pp. 509-536.
8. Culick, F. E. C., and Yang, V., "Prediction of the stability of unsteady motions in solid propellant rocket motors," *Nonsteady Burning and Combustion Stability of Solid Propellants*, Progress in Astronautics and Aeronautics, Vol. 143, ed. L. DeLucs, E. W. Price and M. Summerfield, 1992, pp. 719-779.
9. Zinn, B. T., and Powell, E. A., "Nonlinear Combustion Stability in Liquid-Propellant Rocket Engines," *Thirteenth Symp. (Intl) on Combustion*, 1971, pp. 491-503.
10. Padmanabhan, M. S., Powell, E. A., and Zinn, B. T., "Predicting Nonlinear Axial Instabilities in Solid Rockets Using Exact and Approximate Solution Techniques," *Sixteenth Symp. (Intl) on Combustion*, 1977, pp. 1243-1255.
11. Margolis, S. B., "Nonlinear Stability of Combustion-Driven Acoustic Oscillations in Resonance Tubes," *J. Fluid Mech.*, Vol. 253, 1993, pp. 67-103.
12. Baum, M., and Poinsot, T. J., "Using Direct Numerical Simulations to Study H<sub>2</sub>/O<sub>2</sub>/N<sub>2</sub> Flames with Complex Chemistry," *J. Fluid Mech.*, 1994, to appear.
13. Lele, S. K., "Compact Finite Difference Schemes with Spectral-like Accuracy", *J. Comp. Phys.*, Vol. 103, 1992, pp. 16-42.
14. Poinsot, T., and S. Lele, "Boundary Conditions for Direct Simulation of Compressible Viscous Flows", *J. Comp. Phys.*, Vol. 101, 1992, pp. 104-129.

15. Thompson, K., "Time-dependent Boundary Conditions for Hyperbolic Systems II", *J. Comp. Phys.*, Vol. 89, 1990, pp. 439–461.
16. Mu, S., M. S. thesis, University of Colorado, Boulder, 1994.

### Figure Captions

FIG. 1. Schematic representation of model problem. The mean flow is along the  $x'$ -axis. Acoustic perturbations are imposed at  $x' = 0$ . Non-reflecting boundary conditions are imposed at  $x' = L$ .

FIG. 2. Equally spaced contour lines of  $100(T - T_\infty)/T_\infty$  at  $t = 25$ ,  $Re = 2000$

FIG. 3. Acoustic pressure time history at  $x = 0.6$ , at wall (solid line) and center (dashed line).  $\Omega = 10$ , mesh =  $81 \times 81$  and  $Re = 20000$ .

FIG. 4. Amplitudes of (a) zeroth and (b) first transversal spatial mode component of acoustic pressure for  $\Omega = 10$ , mesh =  $81 \times 81$  and  $Re = 20000$ .

FIG. 5. Acoustic pressure time history at  $x = 0.15$ , center (dashed) and wall (solid) for  $\Omega = 40$ , and  $Re = 20000$ .

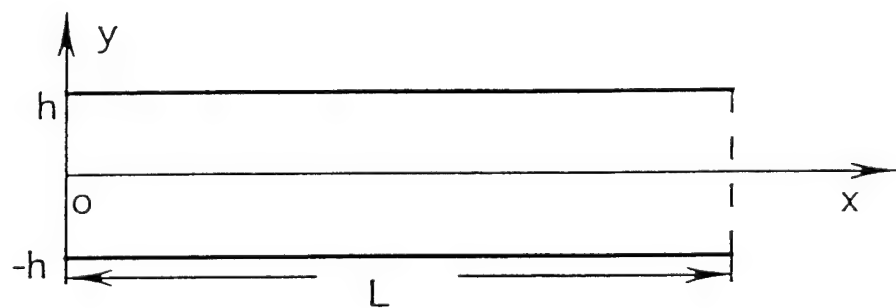
FIG. 6. Amplitudes of (a) zeroth and (b) first transversal spatial mode component of acoustic pressure for  $\Omega = 40$ , and  $Re = 20000$ .

FIG. 7. Acoustic pressure time history at different locations. “c”: centerline; “w”: wall. (1)  $x = 0.1$ , (2)  $x = 0.2$ , (3)  $x = 0.3$ , (4)  $x = 0.4$ , (5)  $x = 0.5$ , (6)  $x = 0.6$ , (7)  $x = 0.7$ , (8)  $x = 0.8$  for  $\Omega = 10\pi$ , and  $Re = 20000$ . Note acoustic time scale is 0 to 4 (0 to 140 in the time scale used by Wang and Kassoy), and scale for acoustic pressure is -5 to 5 in all the figures

FIG. 8. Acoustic pressure contours (equispaced) at (a)  $t = 3.0$ , (b)  $t = 3.05$ , (c)  $t = 3.10$ , (d)  $t = 3.14$  for  $\Omega = 10\pi$ , and  $Re = 20000$ .

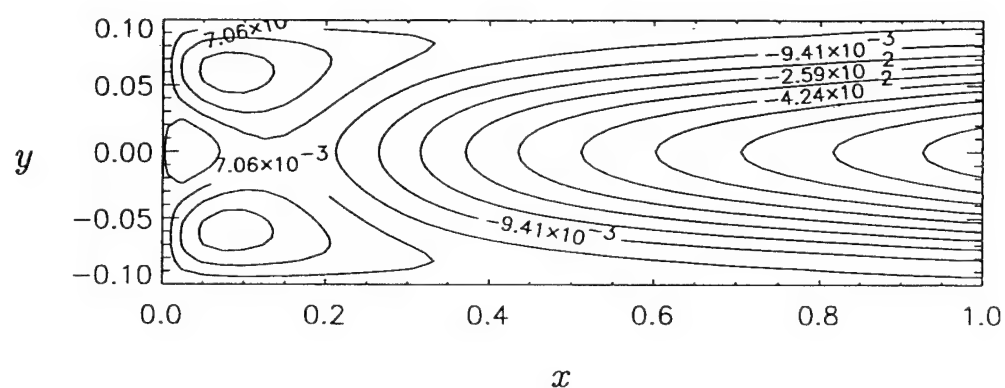
FIG. 9. Axial acoustic velocity profiles at  $x = 0.5$  and (a)  $t = 3.00$ , (b)  $t = 3.14$ , (c)  $t = 3.30$ , (d)  $t = 3.45$ , (e)  $t = 3.62$  for  $\Omega = 10$ , mesh =  $81 \times 161$  and  $Re = 20000$ . Note  $u$  axis scale is -0.6 to 0.6, and  $y$  axis scale is -0.1 to -0.080.

Mu & Mahalingam  
Fig 1



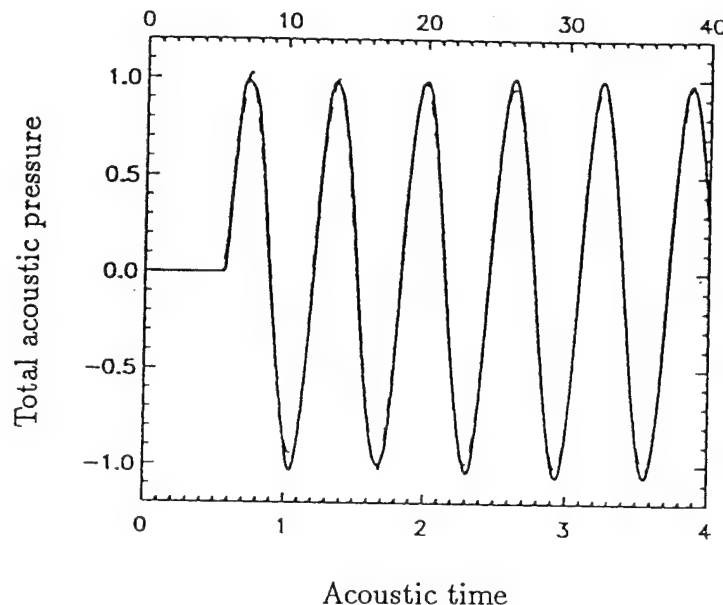
Mu & Mahalingam

Fig 2



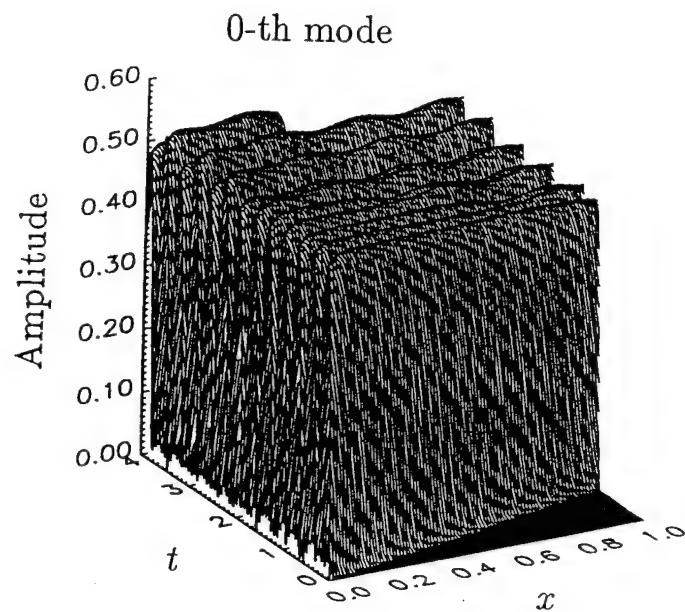
Mu & Mahalingam  
Fig 3

Time scale used by Wang and Kassoy

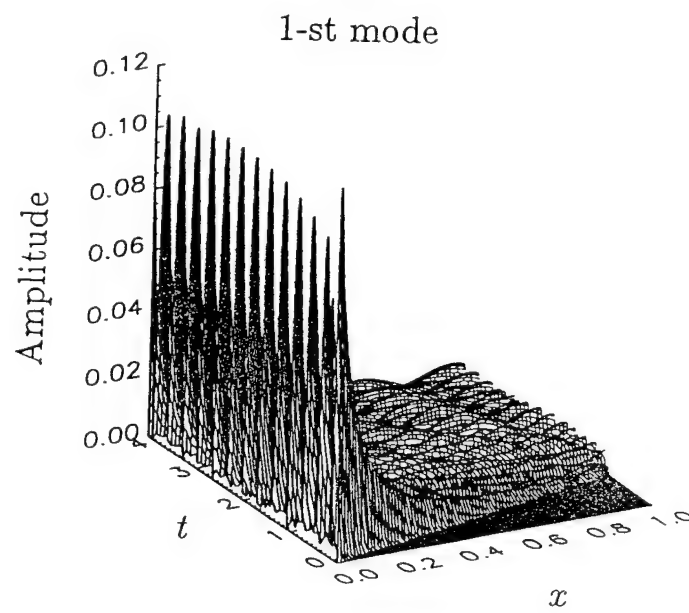


*Mu & Mahalingam*  
*Fig 4*

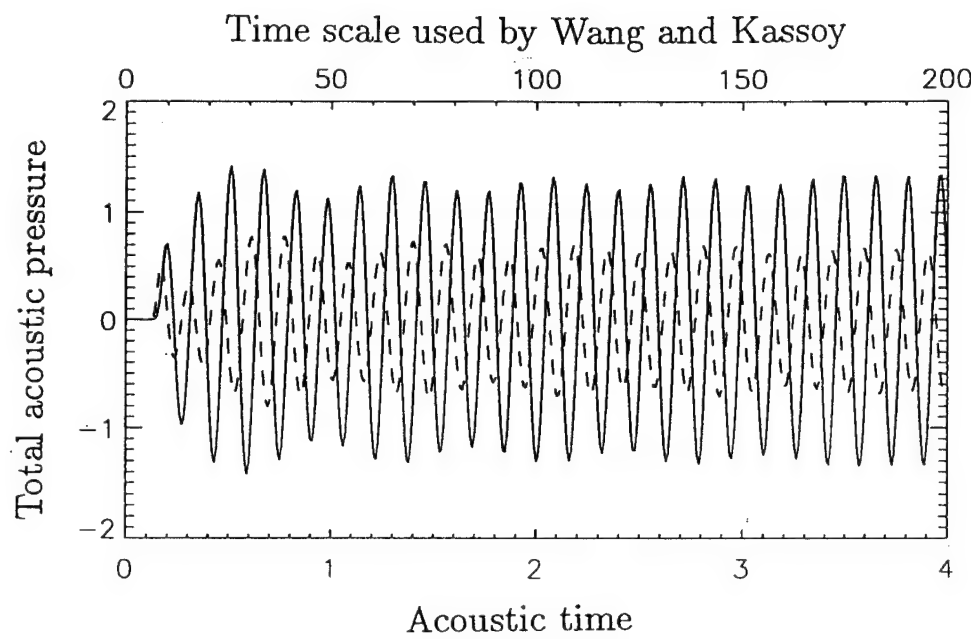
(a)



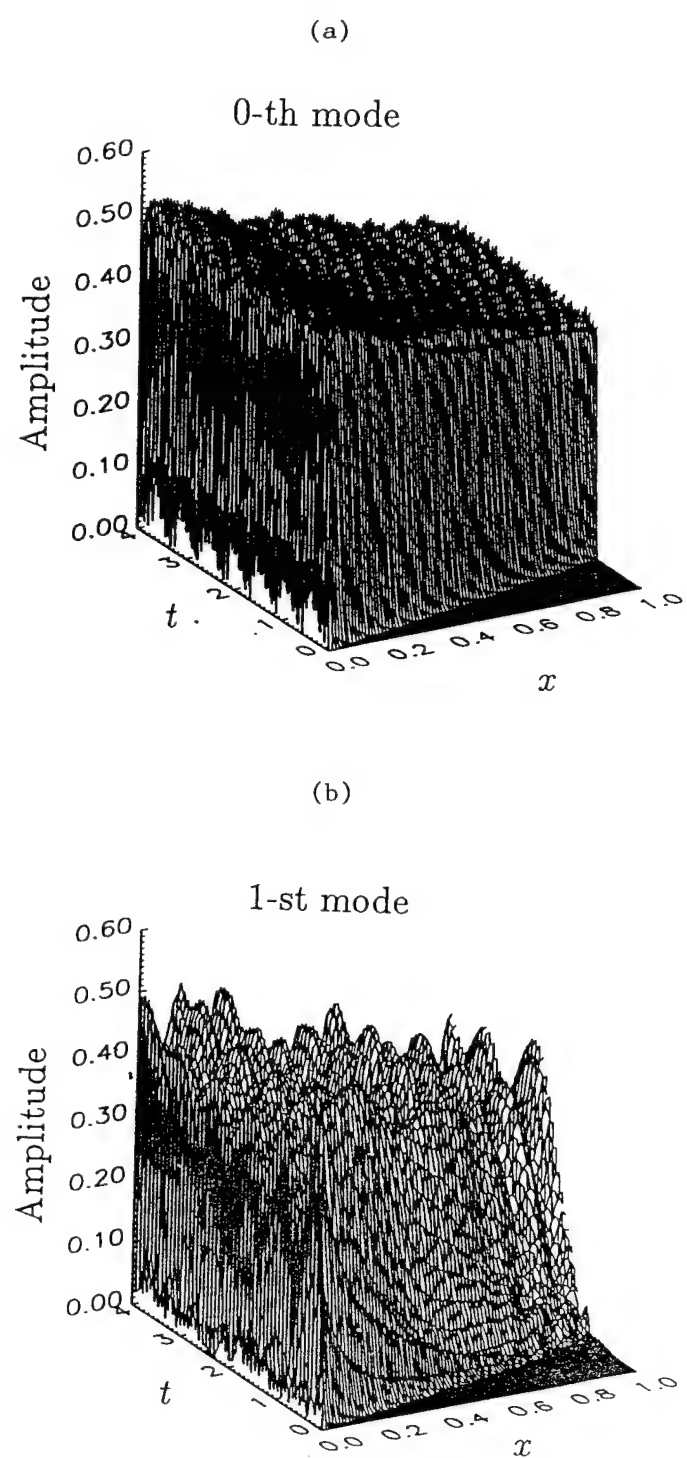
(b)



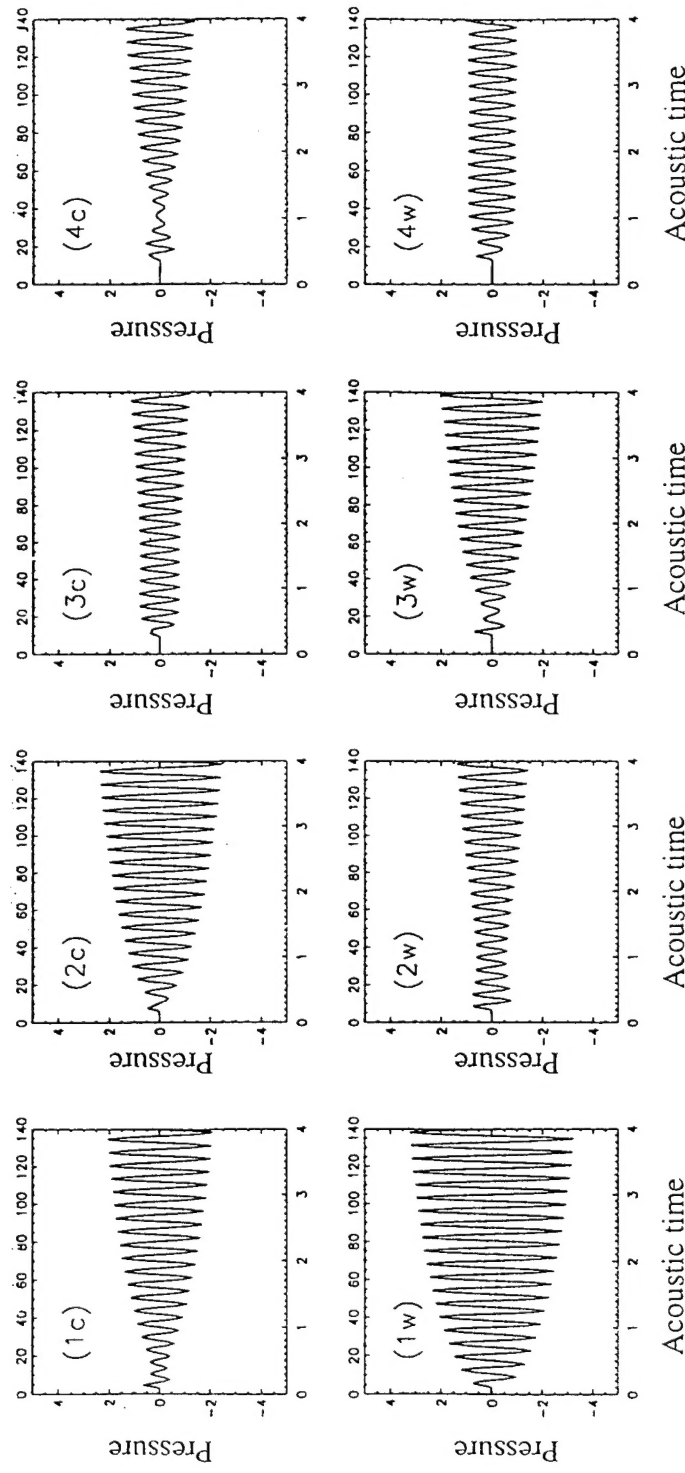
Mu  $\xi$  Mahalingam  
Fig 5



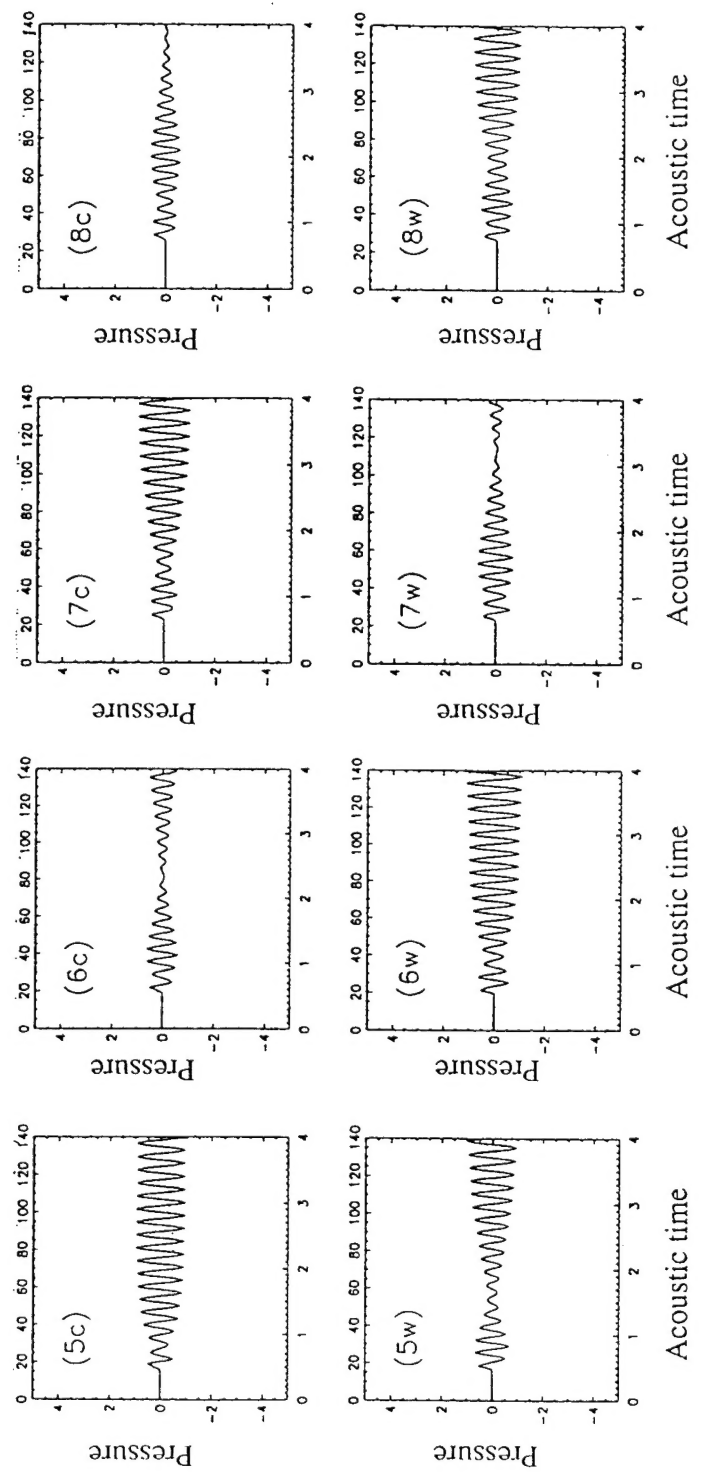
Mu & Mahalingam  
Fig 6



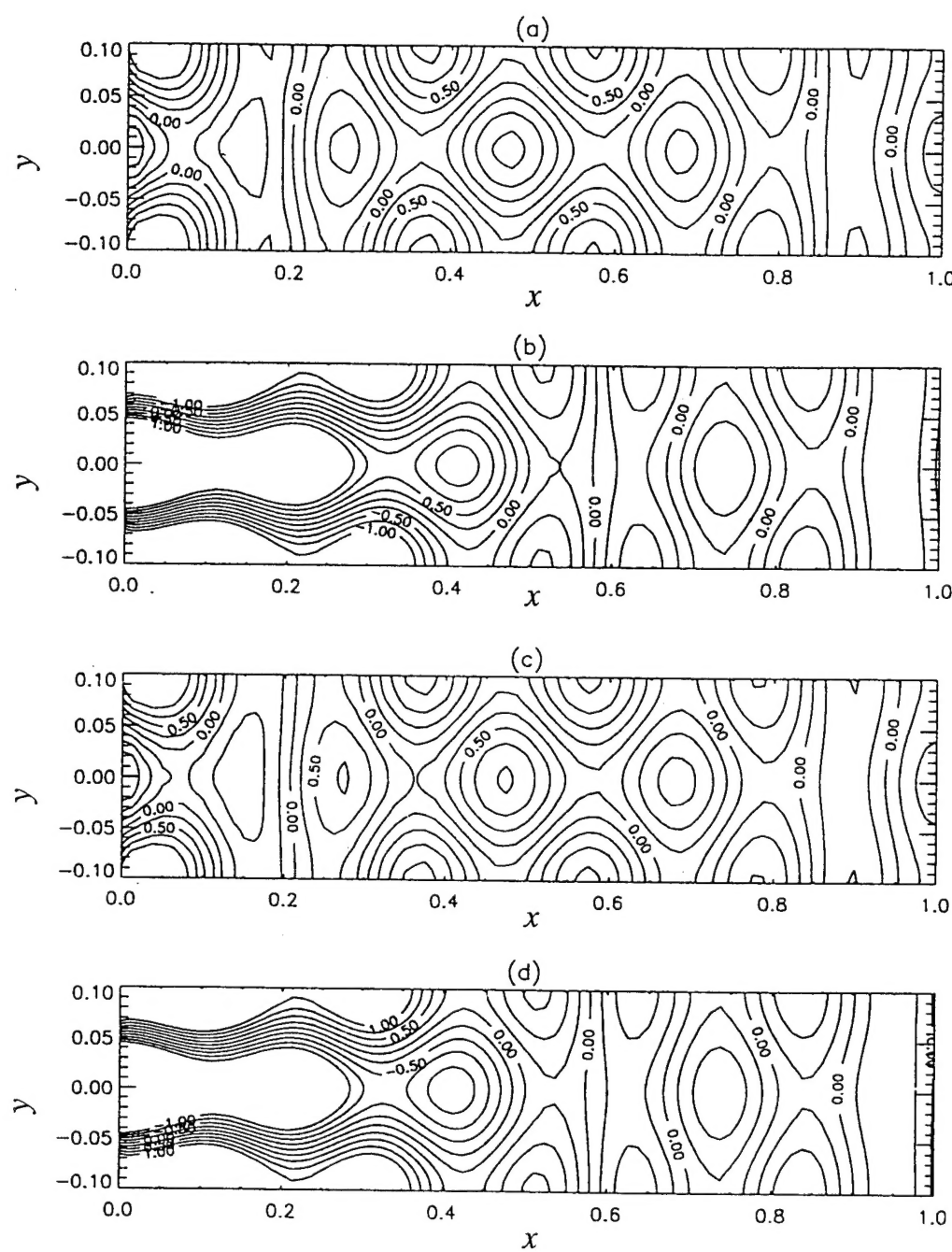
Mus & Mahalingam  
Fig 7



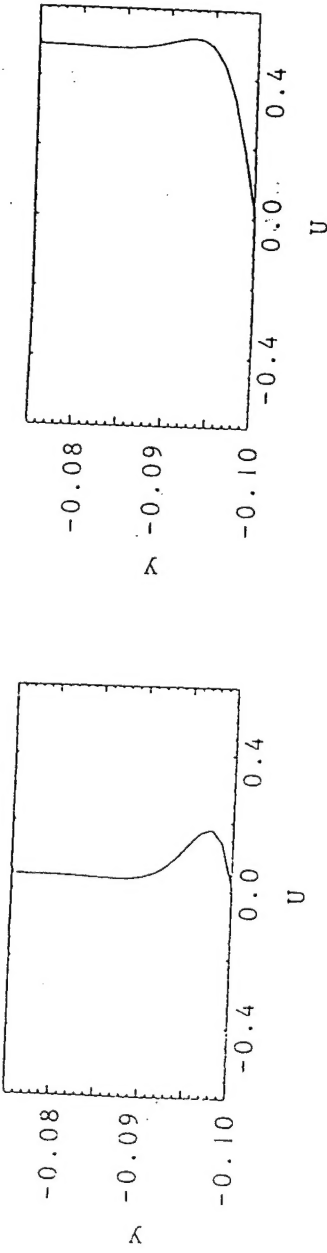
Mu & Mahalingam  
Fig 7 (Cont'd)



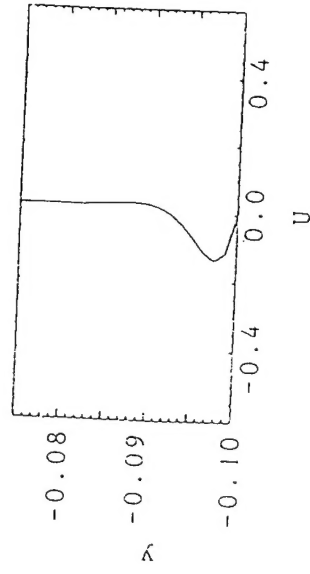
Mu & Mahalingam  
Fig 8



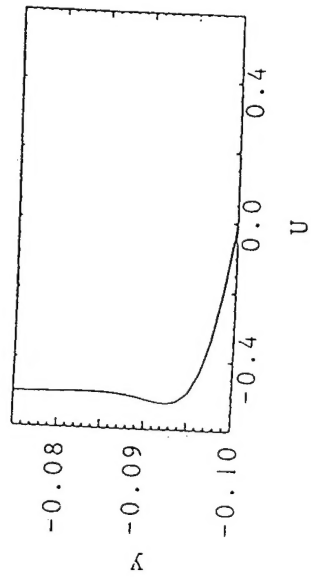
(b)



(c)



(d)



(e)

